NUCLEAR SCIENCE AND ENGINEERING: **132**, 155–180 (1999)

On the Propagation of Rays in Discrete Ordinates

Kirk A. Mathews*

Air Force Institute of Technology, AFIT/ENP, 2950 P Street – Building 640
Wright-Patterson Air Force Base, Ohio 45433-7765

Received May 14, 1998
Accepted October 19, 1998

Abstract—*Discrete ordinates calculations are presumed to translate particles from cell to cell in the directions specified in the angular set. This should result in uncollided particles from a small source propagating through the spatial mesh in narrow beams in these directions. Accurate high-order angular quadratures presume accurately attenuated propagation in the intended directions. This work examines the ability of various spatial quadratures to propagate rays correctly. Some widely used methods are shown to fail at this fundamental task. Diamond-difference approximations introduce undamped lateral oscillations, resulting in severely unphysical flux representations. Nonlinear fixups can prevent negativity but do not correct the underlying failure to properly propagate rays. First-moment conserving schemes tend to be successful but can be degraded in performance by simplifying approximations that are often used. Characteristic schemes are shown to have significant advantages. New characteristic methods are developed here that are exact (in a certain sense) in propagating rays and that uncouple the calculation of adjacent spatial cells in the mesh sweep. This enables DO loops to be converted to DO INDEPENDENT loops, with obvious implications for vector and/or parallel implementations.*

I. INTRODUCTION

The fundamental concept of discrete ordinates radiation transport calculations is that particles are modeled as streaming only in specified, discrete directions from collision to collision. This stems from a vision of the transport equation, discretized in angle but not in space. In an actual discrete ordinates calculation, discretized in space, particles should propagate through the mesh in narrow rays, in the correct directions, properly attenuated. Whether this is achieved depends on the properties of the spatial quadrature in ways that are not at all obvious. We show here that some widely accepted methods fail rather badly at this fundamental task, while other less-used methods are much more successful. Two new methods are developed that are exact in the propagation of rays with respect to measures of performance that are defined as follows.

We use the term *spatial quadrature* in preference to the more-often-used terms *spatial differencing* and *spatial discretization*. We use spatial discretization in reference to partitioning the spatial domain of a problem into a mesh of cells. Spatial differencing seems to have an implicit assumption that a divided difference approach is used, whereas spatial quadrature arises from the more general viewpoint that the essential process is the integration of the $\hat{\Omega}\cdot\vec{\nabla}+\sigma$ operator through the problem domain. This is done in two parts: the integration over each cell and the flow through the boundary between cells. The former is essential to every method, at least in the sense that the divergence theorem leads to the cell balance equation, which is used even in the derivation of the diamond difference (DD) equations. The latter is present in all methods. However, the redistribution of flux along the edge of each cell implicit in passing it from cell to cell can have a significant effect on the propagation of rays, as we show as follows.

For a linear spatial quadrature (in the sense of superposition of solutions), the discrete ordinates solution can be viewed as the superposition of rays of particles extending outward (in all the directions in the angular quadrature set) from each cell that contains emitters or that downscatters particles from higher-energy groups or that scatters particles from the rays that cross the cell. The spatial quadrature algorithm achieves two things: First, it transports particles from sources within the cell through the cell to its boundaries, and second, it

*E-mail: kmathews@afit.af.mil

transports particles entering through some boundaries through the cell to other boundaries, eliminating some of each that collide within the cell. Rays propagate as particles cross through the cells of the mesh. Errors occur in two ways: (a) in approximating the distribution and transport of source particles within the cell and (b) in propagating rays through the mesh. This work focuses on the latter errors. In the propagation of rays, refinement of the mesh decreases the error made in crossing each cell, but more cells must be crossed. Thus, as when integrating ordinary differential equations, the order of global truncation error is one less than the order of the local truncation error. In two- or three-dimensional meshes, ray propagation errors can exhibit qualitatively different behaviors. In particular, what should be a collimated beam of uncollided particles spreads into a broadening fan of particle flow. This effect is often called numerical diffusion. At best, this fan will be narrow and positive (or accompanied by narrow bands of negative flux along its edges), or it may be broad with lateral oscillations. The oscillations may be weakly damped or even undamped. The beam may propagate in the wrong direction, and it may be attenuated inaccurately. This paper examines these behaviors as exhibited by a variety of algorithms.

The discrete ordinates method has been successful largely because these artifacts tend to average out when the rays are all superposed, at least for most application problems. Lathrop[1] examined *ray effect* using complete transport problems, with emission in many cells and scatter in all of them. By that term, he meant that the expected behavior of rays diverging from a localized source could be seen in the discrete ordinates scalar fluxes. Here, we consider ray effect to be a normal property of discrete ordinates and are concerned with other artifacts, such as a ray that travels in the wrong direction. Recently, Petrovic and Haghighat[2] explored the failings of DD-based methods for deep penetration problems with some pure absorber problems in which particles entered the mesh through a portion of one face. Their paper provides an excellent review of the relevant literature, which we will not duplicate here. The work reported here began as an effort to extend their investigation to examine first-moment and characteristic spatial quadratures.

In this work, we examine the propagation of an individual ray of uncollided particles, by which we mean the discrete ordinates solution to a problem in which there are no sources within the mesh, vacuum boundaries on all sides, and incident current only through one face of one cell in one of the discrete ordinates. We found some of these results to be startling and all to be revealing.

Spatial quadrature methods tested include linear, zeroth-moment methods and linear, first-moment methods. Nonlinear methods, including linear methods with fixups, do not provide solutions that are superpositions of stars of rays—no analysis of such methods is attempted, although some examples are presented. Linear, zeroth-order methods, especially characteristic methods, will yield to some analysis.

The analysis and testing performed here is limited to *x-y* geometry with uniform meshes of rectangular cells. Zeroth-moment, linear methods analyzed are DD, step,[3] step characteristic[4] (SC), and a new variant of SC that we call the independent step characteristic (ISC) method. First-moment, linear methods included are linear-linear nodal[5] (LL), linear nodal[6] (LN), linear discontinuous[7] (LD), bilinear discontinuous (BLD), linear characteristic[8] (LC), and the new independent linear characteristic (ILC) method. The effects of fixups on some of these methods are also demonstrated. The BLD method requires cell bilinear flux and source moments and is not, strictly speaking, a first-order method. Nevertheless, we include it with the first-order methods for comparison to LD.

We evaluate the performance of the methods on the basis of cell-edge fluxes rather than cell-center or cell-average fluxes because rays propagate from cell to cell as determined by the cell-edge fluxes and because adjacent region of different composition are coupled through the cell-edge fluxes at the boundary between them. In slab geometry, for example, DD can provide accurate average fluxes in one region but with oscillating cell-edge fluxes that couple to a second region where serious errors in average flux are driven entirely by the error in the cell-edge flux at the boundary between regions. These difficulties are readily avoided (in slab geometry) by using sufficiently fine meshes. In more spatial dimensions, there are more opportunities for unphysical artifacts: rays that propagate in the wrong directions, rays that broaden excessively, rays that are accompanied by undamped oscillations to one side, and so on. These are the focus of this paper. If such artifacts are present, sooner or later arrangements of shapes, orientations, thicknesses, and compositions of objects will arise in practice that exacerbate these artifacts to produce inaccurate engineering results. In our view, a method that has unreliable ray propagation will have unreliable region boundary fluxes and hence unreliable coupling between regions.

II. LINEAR, ZEROTH-MOMENT METHODS

Consider a ray of particles traveling in direction $\hat{\Omega} = \mu\hat{e}_x + \eta\hat{e}_y + \xi\hat{e}_z$ that enters a uniform, rectangular mesh through the bottom face of the lower left cell. To examine the propagation of the uncollided particles in a simple case where it should be a straight beam in a known direction with known attenuation, the source (including scattering source) is set to zero in all the cells, and all cells are the same size, shape, and material. Figure 1 shows the bottom-left cell and the adjacent cell to its right. Without loss of generality, we assume that $0 < \omega_d < \omega < \pi/2$, as shown in Fig. 1. The analytic solution for the flux along the top of these two cells is

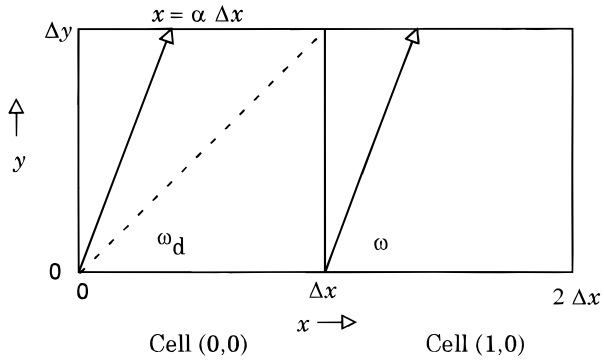

Fig. 1. Bottom-left cells of mesh.

$$\psi(x,\Delta y,\hat{\Omega}) = \begin{cases} \psi(x-\alpha\Delta x,0,\hat{\Omega})e^{-\epsilon_y} \\ \quad \alpha\Delta x < x < (1+\alpha)\Delta x \\ 0 \quad \text{otherwise} \ , \end{cases} \tag{1}$$

where

$$\epsilon_y = \sigma\Delta y/\eta \ ,$$

$$\epsilon_x = \sigma\Delta x/\mu \ ,$$

and

$$\alpha = \epsilon_y/\epsilon_x \ .$$

For any linear, zeroth-moments-only spatial quadrature method, the average flux in the cell,

$$\psi_A = \int_0^{\Delta x} \frac{dx}{\Delta x} \int_0^{\Delta y} \frac{dy}{\Delta y} \psi(x,y) \ , \tag{2}$$

the average source in the cell, S_A, the average flux along the bottom edge,

$$\psi_B = \int_0^{\Delta x} \frac{dx}{\Delta x} \psi(x,0) \ , \tag{3}$$

and the average fluxes along the other edges (defined similarly) are approximated as being linearly related:

$$\psi_A = g_{AB}\psi_B + g_{AL}\psi_L + g_{AS}S_A \ , \tag{4}$$

$$\psi_R = g_{RB}\psi_B + g_{RL}\psi_L + g_{RS}S_A \ , \tag{5}$$

and

$$\psi_T = g_{TB}\psi_B + g_{TL}\psi_L + g_{TS}S_A \ , \tag{6}$$

where the subscripts refer to portions of the cell or to averages over those portions, with: A = cell average, B = bottom face, L = left face, R = right face, and T = top face. The subscript S refers to the contribution due to the source within a cell. Thus, the coefficient g_{TS}, for example, gives the contribution to the average flux over the top face due to a unit source in the cell.

The coefficients g can be functions of the geometric parameters and the cross section but not of the fluxes or source. Nonlinear methods, including fixups such as setting negative fluxes to zero, specify one or more of the coefficients as dependent on the fluxes and/or the source.

Algorithm 1, presented in Appendix A, shows a Fortran-90-style pseudocode listing of a simple discrete ordinates mesh sweep for directions in the first quadrant. The other quadrants are similar but reverse the cell index loop(s) order to sweep from right to left or top to bottom (or both). The SQ subroutine implements Eqs. (4), (5), and (6). DO INDEPENDENT has been used to indicate opportunities for parallel execution. A typical, sequential-execution code would eliminate the n index (for quadrature direction) to minimize storage.

Characteristic methods approximate the spatial moments of the fluxes as those moments of the analytic solution of the Boltzmann transport equation,

$$\mu \frac{\partial\psi(x,y)}{\partial x} + \eta \frac{\partial\psi(x,y)}{\partial y} + \sigma\psi(x,y) = S(x,y) \ , \tag{7}$$

(in the cell and on its outflow edges) with the source and flux on the inflow edges having assumed spatial distributions that match the moments given as input data to the spatial quadrature routine. For example, SC assumes constant fluxes on the inflow edges and a constant source in the cell. Because the flux from the left face cannot reach the right face, characteristic methods have $g_{RL} \equiv 0$ for directions with $0 < \alpha < 1$, as shown. We will refer to any method with this property as a *characteristic-like* method. Stated more generally, in (x,y) geometry, with respect to a given quadrature direction, a cell in the interior of the mesh has four neighboring cells. One is longitudinally upstream, and one is longitudinally downstream. For the example direction, these are the cells below and above the cell in question, respectively. Similarly, one is laterally upstream, and one is laterally downstream. For the example, these are the cells to the left and right, respectively. In (x,y,z) geometry, there are six adjacent cells; two are laterally upstream, and two are laterally downstream. The distinction between lateral and longitudinal faces (or neighbors) is that particles flow across the cell from the longitudinally upstream face to the (opposite) longitudinally downstream face, while particles do not flow across the cell from the longitudinally upstream face(s) to the longitudinally downstream face(s). Characteristic methods exhibit this behavior because of the methodology by which they are derived. Characteristic-like methods could be derived in other ways but would retain these properties. For notational simplicity, and without loss of generality, we presume that the quadrature direction is oriented as in the example ray and refer to the faces and adjacent cells as bottom or below, top or above, left and right.

Using this nomenclature, for the example ray shown in Fig. 1, the bottom face is longitudinally upstream, the top face is longitudinally downstream, the left face is laterally upstream, and the right face is laterally downstream. In sweeping the mesh, only some of the quadrature directions in the first quadrant have this orientation with respect to the cell diagonal. Those for which the left face is longitudinally upstream, and so on, can be treated by an $x \leftrightarrow y$ exchange symmetry in the formulas. One can force characteristic-like methods into the sweep of algorithm 1 by testing the direction cosines inside the SQ routine and performing the exchanges explicitly or through a call to a lower-level subroutine. Much of this overhead can be avoided by providing separate code blocks for directions above and below the cell diagonal, as shown in algorithm 2 (in Appendix B). This approach constrains the mesh, however: All the cells must be of the same size so that each quadrature direction has the same relation to the cell diagonal in every cell of the mesh as in every other cell of the mesh. If the quadrature set includes directions that project onto the cell diagonal, these can be handled the same as those above the diagonal (as in algorithm 2) or as being below the diagonal, or given special case treatment.

II.A. Characteristic-Like Methods

As the flux entering the bottom of the lower-left cell is translated to the top of that cell and the top of the cell to its right, the current through the $y = 0$ plane that it represents is attenuated to a current through the $y = \Delta y$ plane. For a characteristic-like method, the resulting attenuation factor is

$$a \equiv \frac{\psi_{T_{0,0}} + \psi_{T_{1,0}}}{\psi_{B_{0,0}}} = g_{TB} + g_{TL}\, g_{RB} \ . \tag{8}$$

(The flux $\psi_{i,j}$ is the flux in the cell i cells to the right and j cells up from the lower-left cell. With this notation, the cells are indexed starting from 0,0.)

We use two quantitative measures of the performance of a spatial quadrature. The analytic solution has attenuation factor

$$a_{exact} = e^{-\epsilon_y} \ . \tag{9}$$

One of these measures of performance is the accuracy with which a approximates the exact attenuation.

The flux in the analytic solution is displaced to the right by the distance $\alpha \Delta x$ when it is displaced upward by Δy, in the direction with tangent

$$\tau \equiv \tan(\omega) = \frac{\eta}{\mu} \ . \tag{10}$$

The discretized approximation has some flux propagated directly upward, with no translation to the right, while some is translated right by one cell. The weighted-average distance translated to the right is

$$\overline{\Delta i} \Delta x = \frac{g_{TL}\, g_{RB}}{a} \Delta x \ , \tag{11}$$

resulting in an effective direction of motion ω_{eff}, the tangent of which is

$$\tau_{eff} = \tan(\omega_{eff}) = \frac{\Delta y}{\overline{\Delta i} \Delta x} = \frac{\tau_d}{\overline{\Delta i}} \ , \tag{12}$$

where $\tau_d \equiv \tan(\omega_d) = \Delta y / \Delta x$. Our second measure of performance is the accuracy with which τ_{eff} approximates τ. A family of methods that provide exact performance by these measures could be constructed by using the balance equation

$$\psi_T - \psi_B + \alpha(\psi_R - \psi_L) + \epsilon_y \psi_A = S_A \frac{\Delta y}{\eta} \ , \tag{13}$$

together with auxiliary equations that require $\tau_{eff} = \tau$, $g_{RL} = 0$, and $a = a_{exact}$ to determine the coefficients associated with the entering fluxes. These lead to the conditions

$$g_{TB} = (1 - \alpha) e^{-\epsilon_y} \tag{14}$$

and

$$g_{TL}\, g_{RB} = \alpha e^{-\epsilon_y} \ . \tag{15}$$

One degree of freedom, for example, the ratio $r = g_{TL}/g_{RB}$, remains to be specified. Also, auxiliary relations are needed for the source coefficients. We return to this idea in the following.

Of the flux that a linear, characteristic-like, zeroth-moment methods translates up one row, the fraction

$$p = \frac{g_{TL}\, g_{RB}}{a} = \frac{\tau_d}{\tau_{eff}} \tag{16}$$

is translated right one cell, and the fraction $1 - p$ is translated straight up. As this is repeated from row to row, the lateral distribution (across the cells of the left portion of the row) is a binomial distribution

$$\frac{\psi_{B_{i,j}}}{\sum_{i=0}^{j} \psi_{B_{i,j}}} = \begin{cases} \dfrac{j!}{i!(j-i)!}\, p^i (1-p)^j & i \le j \\ 0 & i > j \ . \end{cases} \tag{17}$$

Figure 2 is a plot of this distribution on a 50×50 mesh, for an example ray, described in Sec. II.A.2. For p not too close to 0 or 1 and j not too small, the binomial is accurately approximated by a Gaussian distribution with mean $\overline{\Delta i} = jp$ and variance $p(1-p)j$. The variance of the distribution of the flux, considered as a piecewise constant distribution in x, is

$$\sigma_j^2 = (\Delta x)^2 \left[\frac{1}{12} + p(1-p)j \right] \ . \tag{18}$$

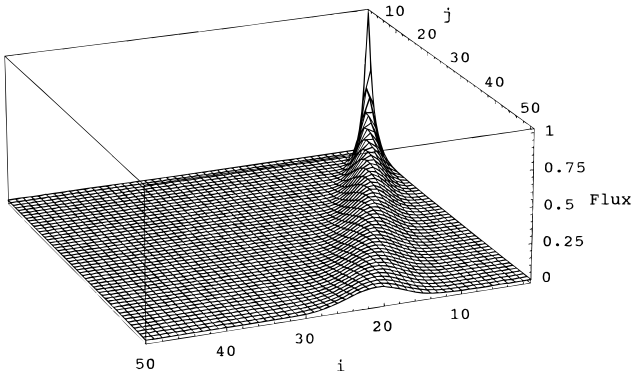

Fig. 2. Example ray as propagated by an exact, zeroth-moment method, such as the ISC method.

The full-width at half-maximum (FWHM) of this Gaussian distribution is

$$w_j = 2.38482\Delta x \sqrt{\frac{1}{12} + p(1-p)j} \ . \tag{19}$$

All linear, characteristic-like, zeroth-moment spatial quadratures that propagate a ray in the same direction have the same value of p and thus the same ray spreading. The example ray, in Fig. 2, has FWHM = 8.30 cells. For such a method to propagate rays exactly, it must have $p = \tau_d/\tau_{eff} = \tau_d/\tau = \alpha$.

II.A.1. Step Characteristic Method

The formulas for the SC method are

$$\begin{aligned}\psi_A = {} & \psi_B[(1-\alpha)\mathcal{M}_0(\epsilon_y) + \alpha\mathcal{M}_1(\epsilon_y)] \\ & + \psi_L[\alpha\mathcal{M}_1(\epsilon_y)] \\ & + S_A \frac{\Delta y}{\eta}[(1-\alpha)\mathcal{M}_1(\epsilon_y) + \alpha\mathcal{M}_2(\epsilon_y)] \ ,\end{aligned} \tag{20}$$

$$\psi_R = \psi_B[\mathcal{M}_0(\epsilon_y)] + S_A \frac{\Delta y}{\eta}[\mathcal{M}_1(\epsilon_y)] \ , \tag{21}$$

and

$$\begin{aligned}\psi_T = {} & \psi_B[(1-\alpha)e^{-\epsilon_y}] + \psi_L\alpha\mathcal{M}_0(\epsilon_y)] \\ & + S_A \frac{\Delta y}{\eta}[(1-\alpha)\mathcal{M}_0(\epsilon_y) + \alpha\mathcal{M}_1(\epsilon_y)] \ ,\end{aligned} \tag{22}$$

where the one-dimensional exponential moments functions are defined as

$$\mathcal{M}_n(\epsilon) = \int_0^1 (1-u)^n e^{-\epsilon u}\, du \ . \tag{23}$$

These functions can be reduced to elementary functions by integrating symbolically, but we use this notation because the resulting formulas are badly conditioned for small ϵ. Algorithms for accurate numerical evaluation of the exponential moments functions needed here have been presented previously.[9]

The attenuation factor for SC is

$$a_{\rm SC} = (1-\alpha)e^{-\epsilon_y} + \alpha[\mathcal{M}_0(\epsilon_y)]^2 \ . \tag{24}$$

Expanding the error in a Maclaurin series:

$$a_{\rm SC} - a_{exact} = \frac{\alpha}{12}\epsilon_y^2 + O(\epsilon_y^3) \ . \tag{25}$$

This is the local truncation error in the propagation of rays by SC, so the global error of the method can be no better than $O(\epsilon_y)$, and indeed, SC is well known to be a first-order method.

The tangent of the ray direction for the SC method is

$$\tau_{eff}^{\rm SC} = \tau\left[(1-\alpha)\frac{e^{-\epsilon_y}}{[\mathcal{M}_0(\epsilon_y)]^2} + \alpha\right] \ , \tag{26}$$

and a series expansion yields

$$\tau_{eff} - \tau = (\tau_d - \tau)\frac{\epsilon_y^2}{12} + O(\epsilon_y^3) \ . \tag{27}$$

Thus, SC propagates rays in directions turned toward the cell diagonal. Comparison of these errors with those of other methods follows.

II.A.2. Example Problem for Ray Propagation

The following problem is used here to demonstrate the propagation of a single ray as achieved by various spatial quadratures. The direction of the ray is taken from the level-symmetric S_4 quadrature set. The mesh is a 50×50 array of identical square cells with vacuum boundaries on all sides. The problem parameters are

$$\begin{array}{lll} \mu = 0.3500212 & \eta = 0.8688903 & \tau = 2.48239 \\ \Delta x = 0.5 & \Delta y = 0.5 & \tau_d = 1 \\ \sigma = 1 & \sigma_s = 0 & \alpha = 0.402837 \\ \epsilon_x = 1.42848 & \epsilon_y = 0.575447 & \xi = 0.3500212 \ . \end{array} \tag{28}$$

The incident fluxes on the left and bottom boundaries of the mesh are zero everywhere except for the bottom face of the lower-left cell, where $\psi_{B_{0,0}} = 1$.

Figure 2 shows the ray produced by any exactly propagating, linear, zeroth-moments, characteristic-like method, that is, any method with $p = \alpha$ and $a = a_{exact}$. The plot shows $\psi_{B_{i,j}}$, normalized as in Eq. (17), for $i = 0$ to 50 and $j = 0$ to 49, with $\psi_{B_{i,50}}$ being the flux at the top edge of the 50th row; however, the plotting routine we used offset the indexes by one, to start at (1,1) instead of (0,0). With this normalization, the decrease in intensity is a consequence only of the lateral spreading of the ray and is not caused by attenuation by

absorption. The viewpoint is chosen so that a ray propagating in the exactly correct direction would enter the mesh at the back right corner and flow directly toward the viewer, emerging from the near edge of the mesh at $i = 1 + \overline{\Delta i} = 1 + 50\alpha = 21.14$. The FWHM of the ray from a linear, zeroth-moment, characteristic-like quadrature method that propagated in the correct direction would be 8.30 cells, by Eq. (19). This orientation of the plot facilitates comparison of the direction, straightness, and spreading of the ray. This same form of plot for each of the methods tested follows. Where needed to make the ray visible, the plot is rotated 90 deg.

II.A.3. Behavior of the SC Method

Figure 3 shows the ray produced by the SC method for this problem. The foregoing analysis indicates that the SC method should propagate the ray, emerging at $i = 21.47$, with FWHM = 8.32 cells. Figure 3 shows a straight, smoothly broadening ray in this direction, with the expected width. The attenuation of a method can be evaluated by examining the attenuation ratio for propagation across j rows of cells:

$$\rho_j = \left(\frac{a_{method}}{a_{exact}} \right)^j \quad . \tag{29}$$

For SC, this ratio is $\rho_{50}^{SC} = 173$, which can be obtained from the fluxes at the top of the top row, or from Eqs. (9) and (24). The SC method overestimates the flux penetrating through the mesh. This occurs when the flux at the right side of a cell, which is an exponentially decreasing function of y, is replaced by a constant value (its average) as the flux entering the left side of the cell to its right. This leveling of the flux has the net effect of moving it upward along the face between the cell and its laterally downstream neighbor. This increase affects the flux reaching the top of the cell to the right but not the flux reaching the top of the cell. This shifts the effective propagation direction toward the cell diagonal, as observed. Thus, the redistribution along the right edge is responsible for both forms of error made by SC in propagating rays. This observation motivated our development of the step adaptive, linear adaptive, and exponential characteristic nonlinear methods in the past.[9–14] Here, it helps to motivate the development of the independent characteristic schemes in Sec. IV.

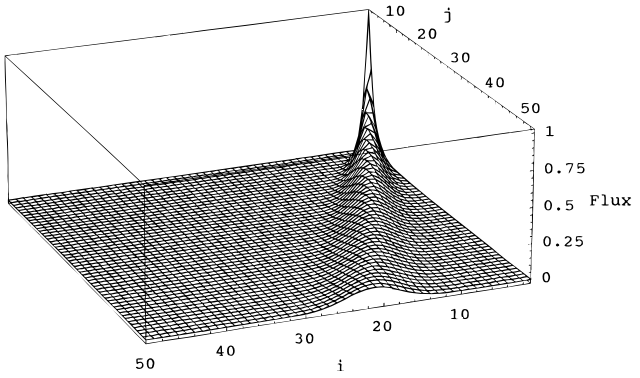

Fig. 3. The SC method.

II.B. Other Methods

Zeroth-moment linear methods that are not characteristic-like spread the flux across the entire row after moving up only one row. So, the narrowest linear, zeroth-moment method rays that can be obtained are for the characteristic-like methods. As is demonstrated in Sec. III, linear first-moment methods can provide decreased ray spreading. The attenuation is readily defined as the ratio of the flux reaching the top of the bottom row of cells divided by that entering the row, namely, that entering through the bottom of the leftmost cell:

$$a = \frac{\sum_{i=0}^{\infty} \psi_{T_{i,0}}}{\psi_{B_{0,0}}} = g_{TB} + g_{TL} g_{RB} \sum_{i=0}^{\infty} (g_{RL})^i \quad . \tag{30}$$

Presuming $|g_{RL}| < 1$, so that the sum converges, the attenuation is

$$a = g_{TB} + \frac{g_{TL} g_{RB}}{1 - g_{RL}} \quad , \tag{31}$$

and the effective direction of motion can be defined using

$$\overline{\Delta i} = \frac{\sum_{i=0}^{\infty} i \psi_{T_{i,0}}}{\sum_{i=0}^{\infty} \psi_{T_{i,0}}} = \frac{g_{TL} g_{RB}}{a(1 - g_{RL})^2} \tag{32}$$

in Eq. (12) to obtain

$$\tau_{eff} = \tau_d \frac{(1 - g_{RL})^2}{1 - \frac{g_{TB}}{a}} \quad . \tag{33}$$

These methods are not necessarily positive; for example, the step method is positive, and DD is not. In evaluating the width of a ray, oscillatory parts can be considered part of the ray. One way to characterize the width is by the FWHM of the Gaussian distribution that has the same mean and variance as the distribution of the absolute value of the top edge fluxes along the edge of the cell. Formulas for this in terms of the g coefficients cannot be simplified (unless the method is positive), so we will examine ray spreading qualitatively from the following plots.

II.B.1. Step Method

We examine the performance of the step method not because it is in any way a contender for actual use but

rather because it is well known to be inaccurate, and it is instructive to visualize how it fails in propagating a single ray. The step method is defined by using the particle balance equation and approximating the flux throughout the cell and on its outflow faces as constant, yielding

$$\psi_A = \psi_R = \psi_T = \frac{\psi_B + \alpha\psi_L + S_A \dfrac{\Delta y}{\eta}}{1 + \alpha + \epsilon_y} \ . \tag{34}$$

The attenuation simplifies to

$$a_{Step} = \frac{1}{1 + \epsilon_y} \ . \tag{35}$$

The series expansion of the local truncation error is

$$a_{Step} - a_{exact} = \frac{\epsilon_y^2}{2} + O(\epsilon_y^3) \ , \tag{36}$$

leading to first-order global error. The tangent of the effective propagation direction is

$$\tau_{eff}^{Step} = \tau(1 + \epsilon_y) \ , \tag{37}$$

which has first-order error. In this case, the ray is turned away from the cell diagonal, toward the *y* axis, as can be clearly seen in Fig. 4, where it emerges spread across cells 6 through 20 rather than being centered on cell 21. The S_4 ray has $\tau_{eff}^{SC} = 3.9$ as compared to $\tau = 2.48$. Even though this is not a characteristic-like method, the ray is not significantly wider than the SC ray; its FWHM is ~9. Step overestimates the flux penetrating the 50 rows by a factor of 374.

II.B.2. Diamond Difference

The DD method has been widely used because of its low computational cost per cell and its second-order global truncation error. It is derived by combining the cell balance equation with the auxiliary approximations $\psi_B + \psi_T = 2\psi_A = \psi_L + \psi_R$, yielding

$$\psi_A = \frac{2\psi_B + 2\alpha\psi_L + S_A \dfrac{\Delta y}{\eta}}{2 + 2\alpha + \epsilon_y} \ , \tag{38}$$

$$\psi_R = \frac{4\psi_B + (2\alpha - 2 - \epsilon_y)\psi_L + 2S_A \dfrac{\Delta y}{\eta}}{2 + 2\alpha + \epsilon_y} \ , \tag{39}$$

and

$$\psi_T = \frac{(2 - 2\alpha - \epsilon_y)\psi_B + 4\alpha\psi_L + 2S_A \dfrac{\Delta y}{\eta}}{2 + 2\alpha + \epsilon_y} \ . \tag{40}$$

The resulting attenuation factor is

$$a_{\mathrm{DD}} = \frac{2 - \epsilon_y}{2 + \epsilon_y} \ . \tag{41}$$

The error in this Padé expansion for the exponential is

$$a_{\mathrm{DD}} - a_{exact} = \frac{-\epsilon_y^3}{12} + O(\epsilon_y^4) \ , \tag{42}$$

resulting in the well-known second-order global truncation error of the DD method. It is worth noting that $-1 < g_{RL} < 0$ for $0 < \alpha < 1$ regardless of the optical thickness of the cells. Thus, the ray will tend to alternate in sign from cell to cell laterally. This applies to the cell-average fluxes resulting from the ray (of uncollided particles) as well as to the boundary fluxes. What is not obvious is whether these lateral oscillations are stable as the ray propagates longitudinally, from row to row. Figure 5 shows the ray as propagated by DD for the test problem. The oscillations grow relative to the actual ray; the plot is truncated to the range (−5,5) so that the ray can be seen. The method is not unstable in that the flux values remain bounded. The code does not crash on overflow errors. Nevertheless, the normalized solution is

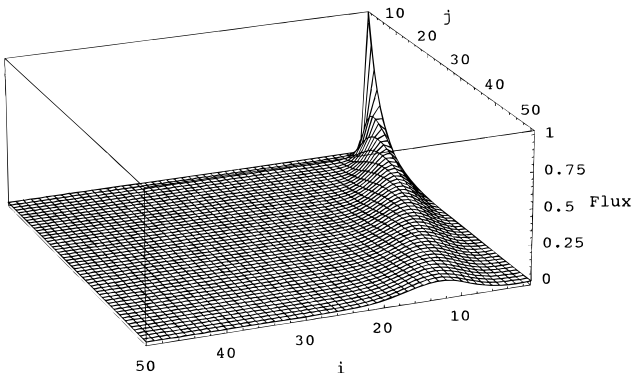

Fig. 4. The step method.

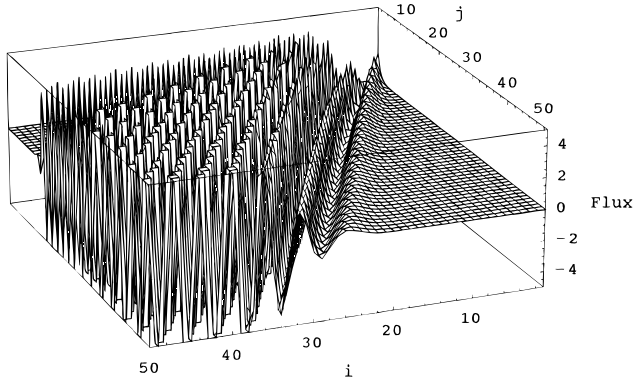

Fig. 5. The DD method (example case).

unstable, with growing oscillations. In fact, the peak oscillations are bounded by the incident flux that gives rise to them but are not significantly attenuated. Figure 6 shows the unnormalized DD solution. The actual ray is rapidly attenuated and would become undetectable in the plot after a few cells. However, an apparent ray of oscillations propagates across the mesh in a direction reflected across the cell diagonal from the true ray.

For the DD method, the average direction of propagation is not a meaningful concept if the ray is accompanied by significant lateral oscillations. Nevertheless, the formula is readily evaluated:

$$\tau_{eff}^{\mathrm{DD}} = \tau\left(1 - \frac{\epsilon_y^2}{4}\right) \quad . \tag{43}$$

Like SC, DD has second-order error in the direction of propagation. For the test problem, $\tau_{eff}^{\mathrm{DD}} = 2.277$, which would be a ray emerging from the mesh at cell 22 rather than 21. In Fig. 5, what appears to be the ray, emerging at about cell 25, is the leading wave of an unstable oscillation. The apparently accurate propagation represented by Eq. (43) belies the reality: The true ray is not even present. Instead, a beam of noise emerges from the side of the mesh at rows 17 through 25, as shown in Fig. 5. This is a beam in the direction with $\tau_{peak\ oscillations}^{\mathrm{DD}} \approx 1/\tau$, that is, in the direction reflected across the cell diagonal.

Figure 7 shows the ray as propagated by DD through the lower-left one-tenth of the test problem, with the mesh refined by a factor of 10 (in both x and y). With $\epsilon_y = 0.0575$, this is a very fine mesh. (In slab geometry, $\epsilon < 0.25$ is sufficiently fine to ensure positivity of DD with even an S_{12} angular quadrature.) The direction of propagation should be correct to nearly four digits. The leading wave appears to be dominant but still is not the intended ray. Also, the oscillations appear to be damped, relative to the ray, but that is an illusion—the onset of instability is outside the mesh but is reached if the entire problem is solved with this resolution. (The plot, however, is too finely meshed to reproduce.) As another way to illustrate this, Fig. 8 shows the lower-left portion of the test problem with a coarser, but still fairly fine, mesh: $\Delta y = \Delta x = 0.2$, so that $\epsilon_y = 0.230$. Again, the waves are damped, decreasing in intensity to the right of where the ray should be. But, in this case, the onset of instability is reached, and the damped waves become unstable farther to the right.

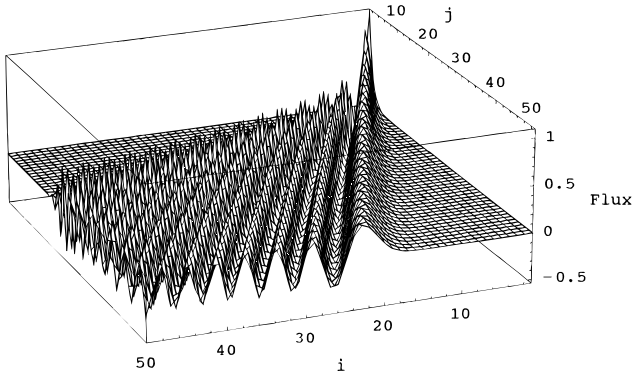

Fig. 7. DD with very fine mesh.

II.B.3. Diamond Difference with Set-to-Zero Fixup

Given the fundamental inability of DD to propagate rays as rays, we find it more surprising that DD does succeed in many application problems than that it fails in others. The simplest fixup for DD is, when computing a cell, to set any negative flux or fluxes produced by DD to zero and recompute the remaining fluxes using the balance equation (and one of the two auxiliary conditions, if appropriate). This is the DZ method. For the example ray, the flux penetrating through the mesh is underestimated by 57%, and the ray is turned toward the diagonal and curves, with τ_{eff}^{DZ} varying from 1.49 to 2.13, as shown in Fig. 9. While the motivation for the fixup is to avoid negative fluxes

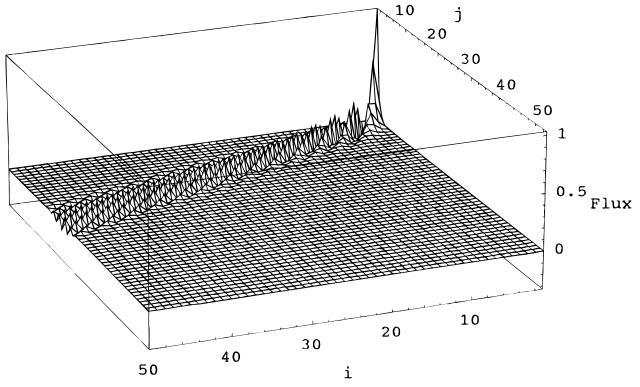

Fig. 6. DD solution—not normalized.

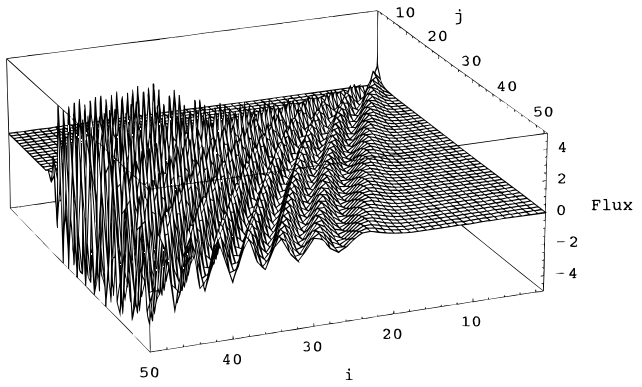

Fig. 8. DD with fine mesh.

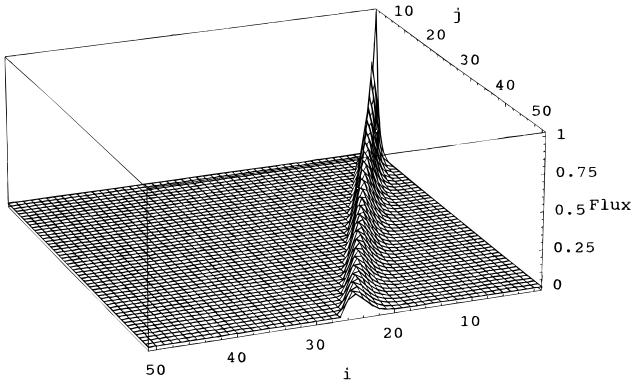

Fig. 9. DD with set-to-zero fixup.

because they are unphysical, the real benefit of the fixup may well be that it renders the method stable.

DZ is one extreme of DD fixups. The step method can be viewed as the other extreme of DD fixup. Recall that the step method overestimates the flux (by a factor of 373 in the example) and turns the ray away from the diagonal, so that the desired behavior lies somewhere between the two. A wide variety of other fixups (theta weighting, directionally dependent weighting, adaptive theta weighting, zero theta weighting, and so on) have been employed in an attempt to retain its faster convergence while ameliorating the unphysical artifacts that sometimes arise from its use. Petrovic and Haghighat provide a good survey of these schemes.[2]

III. FIRST-MOMENT METHODS

First-moment methods conserve first moments as well as zeroth moments. The x first moment of the flux in a cell is

$$\psi_x = \int_0^{\Delta x} \frac{dx}{\Delta x} \int_0^{\Delta y} \frac{dy}{\Delta y}\, 3P_1(x)\psi(x,y) \ , \qquad (44)$$

where $P_1(x) = 2(x/\Delta x) - 1$; ψ_y is defined similarly. The first moment along the top edge is

$$\theta_T = \int_0^{\Delta x} \frac{dx}{\Delta x}\, 3P_1(x)\psi(x,\Delta y) \ ; \qquad (45)$$

the first moments on the other edges are defined similarly. Multiplying the transport equation by $3P_1(x)$ and integrating over the cell leads to the x first-moment balance equation,

$$3\alpha(\psi_R + \psi_L - 2\psi_A) + \theta_T - \theta_B + \epsilon_y\psi_X = S_X \frac{\Delta y}{\eta} \ , \qquad (46)$$

and similarly, the y first-moment balance equation is

$$3(\psi_T + \psi_B - 2\psi_A) + \alpha(\theta_R - \theta_L) + \epsilon_y\psi_Y = S_Y \frac{\Delta y}{\eta} \ . \qquad (47)$$

The balance equations constitute three equations in the seven unknown flux moments, ψ_A, ψ_X, ψ_Y, ψ_T, θ_T, ψ_R, and θ_R. Four auxiliary equations are needed. As with zeroth-moment methods, the balance equations are exact, while the auxiliary equations are approximations, the choice of which defines a method.

First-moment methods use the same mesh sweeps as zeroth-moment methods, with some added complexities. The six first moments (on the edges and over the cell) must be passed to and from the spatial quadrature routine. The boundary conditions must be applied to the first moments. Because $P_1(-x) = -P_1(x)$, the first moments require sign reversals where coordinate reflections are applied. (Note that if 1 and x were used as basis functions, rather than $P_0(x)$ and $P_1(x)$, the zeroth and first moments would be coupled where coordinates are reflected. The separation of variables available with rectangular cells in Cartesian coordinates is essential to this elegance.)

III.A. Nodal Methods

While the term *nodal* finds many uses, here we consider the family of nodal methods introduced by Walters and O'Dell[5] and Walters.[6,7] The basic idea is to multiply the transport equation by $P_0(x) = 1$, or by $3P_1(x)$, and integrate over x. The result is an ordinary differential equation in $\psi(y)$ or $\theta(y)$. The fluxes on the left and right edges appear as forcing functions, approximated as $\psi(0,y) = P_0(y)\psi_L + P_1(y)\theta_L$ and similarly on the right edge. The corresponding moment on the bottom edge, ψ_B or θ_B, is the initial condition. The solution evaluated at $y = \Delta y$ is the corresponding moment at the top edge. This leads to auxiliary equations for ψ_T and θ_T:

$$\psi_T = \epsilon_y\psi_B + \left[S_A \frac{\Delta y}{\eta} + \frac{\psi_L - \psi_R}{\alpha}\right]\mathcal{M}_0(\epsilon_y) + \left[S_Y \frac{\Delta y}{\eta} + \frac{\theta_L - \theta_R}{\alpha}\right][2\mathcal{M}_1(\epsilon_y) - \mathcal{M}_0(\epsilon_y)] \qquad (48)$$

and

$$\theta_T = \epsilon_y\theta_B + \left[S_X \frac{\Delta y}{\eta} + 3\,\frac{2\psi_A - \psi_L - \psi_R}{\alpha}\right]\mathcal{M}_0(\epsilon_y) + 3\,\frac{2\psi_Y - \theta_L - \theta_R}{\alpha}\,[2\mathcal{M}_1(\epsilon_y) - \mathcal{M}_0(\epsilon_y)] \ . \qquad (49)$$

Swapping the roles of x and y leads to the similar equations for ψ_R and θ_R:

$$\psi_R = \frac{\epsilon_y}{\alpha}\psi_L + \left[\frac{S_A}{\alpha}\frac{\Delta y}{\eta} + \alpha(\psi_B - \psi_T)\right]\mathcal{M}_0\left(\frac{\epsilon_y}{\alpha}\right) + \left[\frac{S_X}{\alpha}\frac{\Delta y}{\eta} + \alpha(\theta_B - \theta_T)\right] \times \left[2\mathcal{M}_1\left(\frac{\epsilon_y}{\alpha}\right) - \mathcal{M}_0\left(\frac{\epsilon_y}{\alpha}\right)\right] \quad (50)$$

and

$$\theta_R = \frac{\epsilon_y}{\alpha}\theta_L + \left[\frac{S_Y}{\alpha}\frac{\Delta y}{\eta} + 3\alpha(2\psi_A - \psi_B - \psi_T)\right]\mathcal{M}_0\left(\frac{\epsilon_y}{\alpha}\right) + 3\alpha(2\psi_X - \theta_B - \theta_T) \times \left[2\mathcal{M}_1\left(\frac{\epsilon_y}{\alpha}\right) - \mathcal{M}_0\left(\frac{\epsilon_y}{\alpha}\right)\right] . \quad (51)$$

III.A.1. Linear-Linear Nodal Method

Unfortunately, the unknowns ψ_R and θ_R appear in the nodal auxiliary equations for ψ_T and θ_T, and vice versa. Algebraically uncoupling these equations is not practical without further approximations. With numerical input data, the system can be solved as a linear algebra problem in each cell. This approach makes no further approximations and is called the LL nodal method. Its performance is excellent. Figure 10 shows the test case ray. It has small, strongly damped oscillations to the right side of the ray. The average propagation direction is $\tau_{eff}^{\mathrm{LL}} = 2.4828$, which is nearly exact, and the error in the attenuation through the mesh is negligible: 0.004%. However, because of the computational cost of the linear algebra, the LL method is rarely if ever used. Instead, a DD approximation is used, as described in Sec. III.A.3.

III.A.2. Edge Rotation Fixups

A fixup is often applied to linear first-moments methods to stabilize them and make them strictly positive but nonlinear. The fixup employed by Walters and O'Dell[5] was a negative source rotation fixup in which the first spatial moments of the angular moments of the flux are restricted to not exceed the corresponding zeroth spatial moments. This has negligible cost because it occurs in an outer loop, but it does not stabilize the propagation of rays and so does not guarantee positivity. (In the example problem, the source moments are all zero because the scattering cross section is zero.) To stabilize the ray propagation, an edge rotation fixup (also used by Larsen and Alcouffe with the LC method[8]) can be employed: If $|\theta_R| > \psi_R$, then set $\theta_R = \psi_R \,\mathrm{sgn}(\theta_R)$, and similarly for θ_T. (This presumes that the zeroth moments are positive, which the fixups should ensure.) Note that this method [linear-linear fixup (LLF)] is an ad hoc fixup of LL that violates the conservation of first moments. (First-moment conservation could be restored by using the first-moment balance equation to recompute ψ_X or ψ_Y using the adjusted value of θ_T or θ_R, at considerable cost in complexity and computation. However, this would have no effect on the propagation of rays in pure absorbers.)

As can be expected, the nonlinear fixup degrades the accuracy of the direction of propagation and of the attenuation. LLF has 4% error in attenuation for the example. As shown in Fig. 11, the ray starts out turned toward the diagonal, then turns toward the correct direction as it propagates, with $\tau_{eff}^{\mathrm{LLF}}$ varying from 2.09 to 2.467. (These values were computed from the fluxes. The curvature is difficult to see in Fig. 11.)

III.A.3. Linear Nodal Method

The LN method uses the LL equations but introduces DD approximations for the first moments: $\theta_T + \theta_B = 2\psi_X$ and $\theta_L + \theta_R = 2\psi_Y$. These are not used as replacements for Eqs. (49) and (51) but rather are used to eliminate the final terms of those equations. This

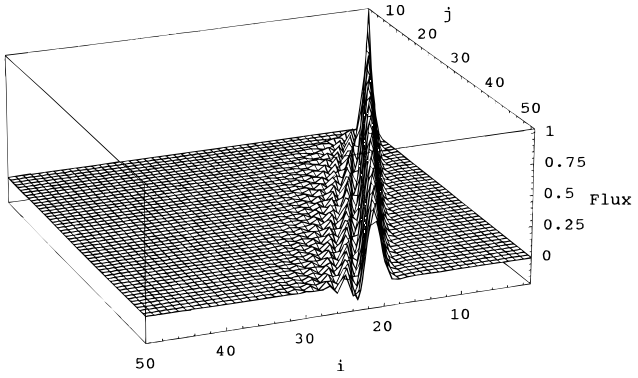

Fig. 10. The LL nodal method.

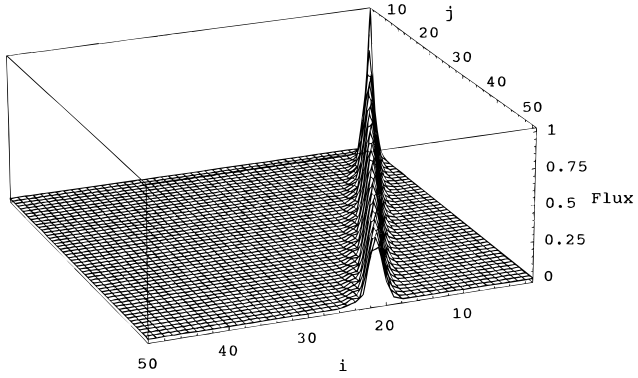

Fig. 11. The LL nodal method with edge rotation fixup.

uncouples the system of seven equations so that they may be written in computationally convenient forms, including casting them in the form of augmented DD equations.[6]

Unfortunately, the DD approximation causes problems. In propagating a single ray, the lateral oscillations that were strongly damped in the LL method can become undamped, relative to the true ray, as is demonstrated by the test problem, shown in Fig. 12. (The mesh is rotated 90 deg to make the ray and the oscillations more clearly visible.) These oscillations dominate the ray, but at least they do decay as they propagate longitudinally through the mesh (unlike those of the DD method). Ignoring the oscillations, the portion of the solution that represents the ray still propagates it in the correct direction, but the error in attenuation through the mesh is increased to +1.3%. The lateral instability seems to have gone unnoticed, perhaps because, as with DD, the average direction of motion and attenuation are not impaired, or perhaps because rotation fixups are routinely employed in practice. Nevertheless, the dominant oscillations mean that the representation of the ray is significantly unphysical.

III.A.4. Linear Nodal Method with Rotation Fixups

Applying the source and edge rotation fixups to the LN method results in the linear nodal fixup (LNF) method. Interestingly, the direction of propagation is not so strongly perturbed with LNF as with LLF: $\tau_{eff}^{\mathrm{LNF}}$ varies from 2.35 to 2.40 for the example ray, shown in Fig. 13. However, the error in attenuation through the mesh is increased to +6%. Lateral oscillations persist along the side of the ray, but they are smaller and are well damped.

III.B. Finite Element Methods

III.B.1. Linear Discontinuous Method

The LD method can be derived directly as a finite element method, similar to the derivations discussed and

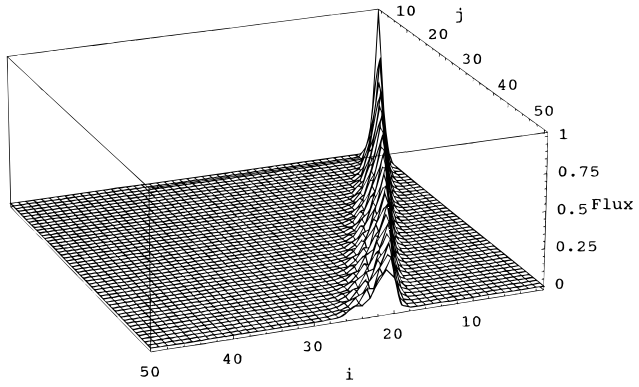

Fig. 13. The LN method with edge rotation fixup.

presented for the BLD method in Sec. III.B.2. It can also be obtained as an approximation to the LL method, as Walters has shown.[6] A step approximation is made for the first moments: $\theta_T = \psi_X$ and $\theta_R = \psi_Y$, and the exponential function is replaced by its Padé(1,2) approximation,

$$e^{-\epsilon} \approx \frac{6 - 2\epsilon}{6 + 4\epsilon + \epsilon^2} \quad , \tag{52}$$

everywhere that it occurs, including in the exponential moments functions, which are readily expressed in terms of the exponential by the recursion: $\mathcal{M}_n(\epsilon) = (1 - n\mathcal{M}_{n-1}(\epsilon))/\epsilon$, with $\mathcal{M}_0(\epsilon) = (1 - e^{-\epsilon})/\epsilon$. The resulting method is linear and has good performance. Figure 14 shows that a ray in almost the right direction, $\tau_{eff}^{\mathrm{LD}} = 2.46$, is accompanied by a fairly large but rapidly damped oscillation to its left. The LD method underestimates the flux reaching row 50 by ~6.5%.

An edge rotation fixup was tested in an attempt to eliminate the oscillations to the left of the ray. This approach was unsuccessful: It resulted in small but weakly damped oscillations on the other side of the ray, and poorer

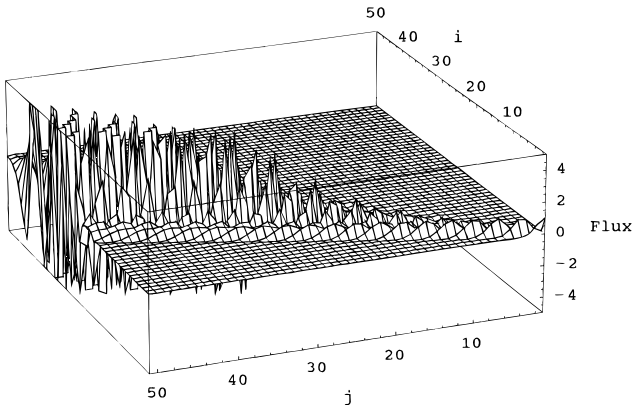

Fig. 12. The LN method.

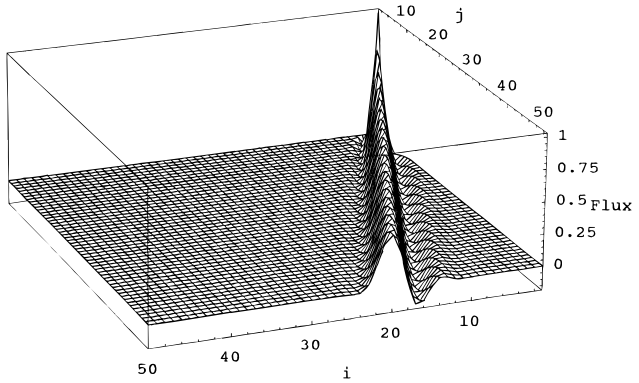

Fig. 14. The LD method.

accuracy. The BLD method, described next, improves beam quality without degrading (or improving) accuracy.

III.B.2. Bilinear Discontinuous Method

The BLD method is similar to LD but includes a bilinear term in the source and flux. Morel, Dendy, and Waring[15] derive the method by expanding the flux in four bilinear basis functions that each evaluate to 1 in one of the corners of the cell and 0 in the other three corners. The corner flux values then determine the cell flux moments and outflow edge moments. Their system of equations is concise and has some elegance, but we were unable to implement it successfully, and we suspect typographical errors. We cast the method in terms of the cell moments and face moments, which has the advantage of facilitating implementation as a direct replacement for other first-moment methods. The only additional modification is to carry the cell bilinear moments,

$$\psi_{XY} = \int_0^{\Delta x} \frac{dx}{\Delta x} \int_0^{\Delta y} \frac{dy}{\Delta y}\, 3P_1(x) 3P_1(y) \psi(x,y) \ , \tag{53}$$

and the corresponding source moments S_{XY} (obtained by angular quadrature of the scattering cross section and flux bilinear moment).

The method is derived by assuming a bilinear expansion of the flux within a cell,

$$\psi(x,y) \approx \psi_A P_0(x) P_0(y) + \psi_X P_1(x) P_0(y) + \psi_Y P_0(x) P_1(y) + \psi_{XY} P_1(x) P_1(y) \ , \tag{54}$$

and linear expansions on each cell edge. Continuity is assumed at the outflow faces but not at the inflow faces (hence the term *discontinuous)*. For flow upward and to the right, the outflow faces are at the top and right, leading to the following continuity equations:

$$\psi_R = \psi_A + \psi_X \ , \tag{55}$$

$$\theta_R = \psi_Y + \psi_{XY} \ , \tag{56}$$

$$\psi_T = \psi_A + \psi_Y \ , \tag{57}$$

and

$$\theta_T = \psi_X + \psi_{XY} \ . \tag{58}$$

These continuity conditions are substituted into the particle and first-moment balances, Eqs. (13), (46), (47), and the bilinear moment balance equation,

$$3\alpha(\theta_R + \theta_L - 2\psi_Y) + 3(\theta_T + \theta_B - 2\psi_X) + \epsilon_Y \psi_{XY} = S_{XY} \frac{\Delta y}{\eta} \ , \tag{59}$$

leading to the linear system

$$\mathbf{L}\vec{\psi} = \vec{q} \ , \tag{60}$$

where

$$\mathbf{L} = \begin{pmatrix} 1+\alpha+\epsilon_y & \alpha & 1 & 0 \\ -3\alpha & 1+3\alpha+\epsilon_y & 0 & 1 \\ -3 & 0 & 3+\alpha+\epsilon_y & \alpha \\ 0 & -3 & -3\alpha & 3+3\alpha+\epsilon_y \end{pmatrix} , \tag{61}$$

$$\vec{\psi} = (\psi_A \quad \psi_X \quad \psi_Y \quad \psi_{XY})^T \ , \tag{62}$$

and

$$\vec{q} = \begin{pmatrix} S_A \dfrac{\Delta y}{\eta} + \alpha\psi_L + \psi_B \\ S_X \dfrac{\Delta y}{\eta} - 3\alpha\psi_L + \theta_B \\ S_Y \dfrac{\Delta y}{\eta} + \alpha\theta_L - 3\psi_B \\ S_{XY} \dfrac{\Delta y}{\eta} - 3\alpha\theta_L - 3\theta_B \end{pmatrix} . \tag{63}$$

This system is solved numerically for the cell flux moments. (Note that **L** is strictly diagonally dominant and so should be well conditioned, unless ϵ_y is very small.) Then the outflow face moments are obtained from the continuity equations.

The BLD method has better ray quality than LD, as is shown in Fig. 15. There is a small negative trough on each side of the ray, but no oscillations are evident. The attenuation of the ray for the example problem is in error by the same 6% as was the case with the LD method.

III.C. Characteristic Methods

III.C.1. Linear Characteristic

The LC method is derived similarly to the SC method, but it assumes first-moment expansions of the source,

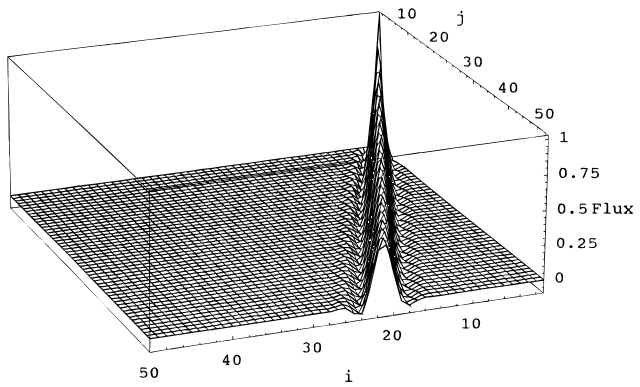

Fig. 15. The BLD method.

$S(x,y) = S_A + S_X P_1(x) + S_Y P_1(y)$, and of the flux along the incident edges, $\psi(x,0) = \psi_B + \theta_B P_1(x)$ and $\psi(0,y) = \psi_L + \theta_L P_1(y)$. The transport equation is integrated along its characteristic lines (particle flow streamlines) to approximate $\psi(x,y)$. The moments of that result, over the cell and over the outflow edges, are obtained by symbolic integration, yielding formulas for the seven unknown flux moments. Each moment, ψ_A, for example, is broken into contributions from the flux entering the bottom, ψ_{AB}, from that entering the left side, ψ_{AL}, and from the source, ψ_{AS}; these contributions sum to ψ_A. Although the LC method is not new, the formulas have not been presented in full before. They are presented in Appendix C, expressed in terms of exponential moments functions.

The zeroth- and first-moment balance equations are implicitly satisfied because the transport equation is exactly satisfied (for the assumed input flux and source moments). They can be used to reduce computational cost (when they are not badly conditioned), or they can be used to check the results of the each cell's calculations for loss of precision or other errors. They are also useful to check the correctness of the formulas.

The LC method performs quite well. Figure 16 shows that the method, although not strictly positive, produces only small and rapidly damped oscillations to the sides of the ray. The propagation direction is nearly correct, $\tau_{eff}^{\mathrm{LC}} \approx 2.482$, and the flux penetrating through row 50 is underestimated by only 0.3%.

III.C.2. Linear Characteristic with Rotation Fixups

The edge rotation fixup described earlier, together with a corresponding source rotation fixup [that restricts the magnitude of ψ_X and ψ_Y to prevent $S(x,y) < 0$ at any point in the cell], renders the LC method strictly positive. Thus, the oscillations to the sides of the ray are eliminated, as shown in Fig. 17. The fixups cause the ray to turn slightly, starting at $\tau_{eff}^{\mathrm{LCF}} \approx 2.30$ and turning toward the correct direction, with $\tau_{eff}^{\mathrm{LCF}} \approx 2.477$. The attenuation is essentially identical to that of the LC method without the fixups.

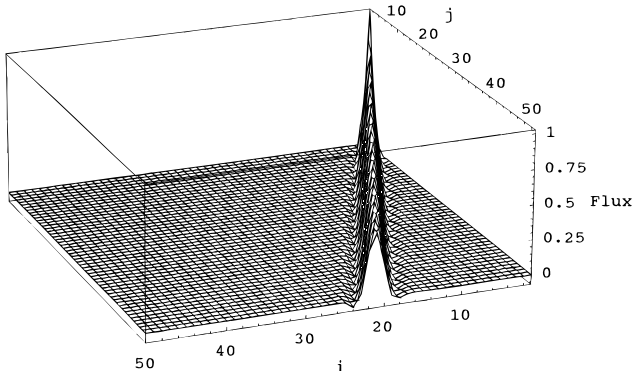

Fig. 16. The LC method.

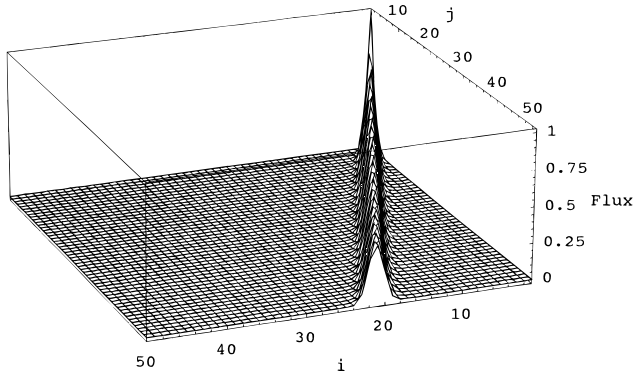

Fig. 17. The LC method with edge rotation fixup.

III.C.3. Approximate LC Method

Larsen and Alcouffe originally proposed an approximation to the LC method presented in Sec. III.C.1 (Ref. 8). For the purpose of obtaining the outflow edge first moments only, they approximated the analytic solution on the outflow edges by certain chords. The details are in Ref. 8. The resulting formulas are

$$\theta_T = e^{-\epsilon_y}[(1 - 3\alpha + 2\alpha^3)\theta_B + 3\alpha(1-\alpha)\psi_B] + \frac{\alpha}{2}\{[2\alpha - 3 + e^{-\epsilon_y}(3 - 4\alpha)]\theta_L + [2\alpha - 3 - e^{-\epsilon_y}(3 - 4\alpha)]\psi_L\} \qquad (64)$$

and

$$\theta_R = \frac{(1-2\alpha)e^{-\epsilon_y} - 1}{2}\,\theta_B - \frac{1 - e^{-\epsilon_y}}{2}\,\psi_B \ . \qquad (65)$$

In their implementation, this saved ~20% in computational costs. As compared to LC, this approximation slightly increases the troughs next to the ray, as shown in Fig. 18; turns the ray more, to $\tau_{eff}^{\mathrm{ALC}} \approx 2.46$; and doubles the attenuation error, to 6.6% at row 50.

III.C.4. Approximate Linear Characteristic Method with Fixups

Adding rotation fixups to the approximate LC method makes it a strictly positive method and removes the negative troughs next to the ray, as shown in Fig. 19. The ray is turned more and is slightly curved, with $2.30 < \tau_{eff}^{\mathrm{ALCF}} < 2.44$, but the attenuation error is essentially the same as without the fixup (6.8%).

IV. INDEPENDENT CHARACTERISTIC METHODS

Error in attenuation and direction of propagation of rays by the SC method arises in the redistribution of flux

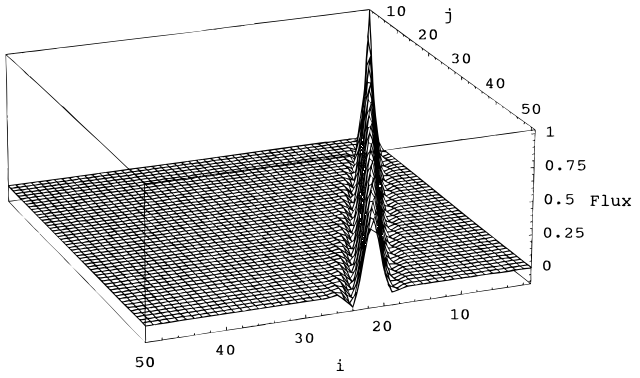

Fig. 18. The approximate LC method.

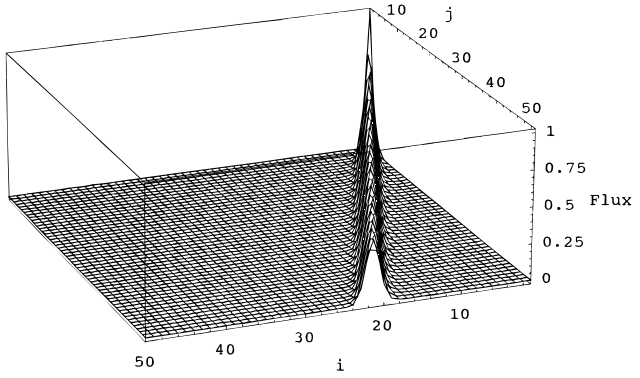

Fig. 19. The approximate LC method with edge rotation fixup.

along the side of each cell. Consider two laterally adjacent cells—one on the left and one on the right. Assuming that the flux enters the bottom of the left cell uniformly distributed along the bottom, as it is represented in the SC method, the uncollided flux that reaches the right edge of the left cell is exponentially distributed along that edge. If the cross sections are the same in the two cells, then the exponentially distributed flux entering the right cell's left face is attenuated with the complementary exponential dependence, resulting in a uniform distribution of the flux along a portion of the top of the right cell. Conventional characteristic methods (SC and LC) introduce error by redistributing the flux as a constant or linear function along the left face of the right cell. That flux results in an exponentially distributed flux along (a portion of) the top edge of the right cell, with an incorrect average value. The flux that enters the bottom of the left cell and reaches the top of that cell is not redistributed in y en route to the top of the cell and so reaches it uniformly distributed in x and properly attenuated. The direction of propagation is distorted because the flux is attenuated correctly in traveling from the bottom to the top of the left cell but is attenuated differently in traveling from the bottom of the left cell to the top of the right cell.

One could, of course, adjust the factor g_{TL} so that the product $g_{RB}g_{TL}$ would have the correct value. Unfortunately, that would distort the influence of the source in the cell. The flux along the right face due to the source within the cell is distributed differently in y than is the flux that entered through the bottom of the cell. Thus, if g_{RB} and g_{RS} are both correctly computed, based on the assumed distribution of the source and entering flux, then a different g_{TL} is needed to obtain the correct product $g_{RS}g_{TL}$. No method can account for these differing distributions along its left face so long as its only input datum is the sum of the fluxes entering through the left face.

IV.A. Independent Step Characteristic Method

A solution to this quandary is to treat some input data for the left cell as input data for the right cell as well. Rather than passing ψ_R exiting the left cell (as returned by one call to the spatial quadrature routine) as ψ_L entering the right cell (as input to another call to that routine), we pass ψ_{BL} and S_{AL}, the bottom flux and average source for the left cell, as inputs to the call to the routine for the right cell, along with the usual ψ_B and S_A that are the flux entering the bottom and average source within the right cell (and cross-section values and geometric parameters for both cells). These extra input data let the method compute directly the two separate contributions to ψ_A and ψ_T due to flux flowing into the cell from its laterally upstream neighbor.

We call the resulting scheme the ISC method because all the cells in a row can be computed in parallel, as shown in algorithm 3 (given in Appendix D). In High-Performance Fortran (HPF), this can be accomplished by applying the !HPF$ Independent directive to either a Do loop or a ForAll loop. We write this simply as DO INDEPENDENT in the algorithms. With traditional schemes, as shown in algorithms 1 and 2 (Appendixes A and B), the spatial sweep proceeds from cell to cell along each row in turn because each cell in the row must await the result of the spatial quadrature as applied to its laterally upstream (as well as its longitudinally upstream) neighbor(s).

In deriving the SC method, the flux in region 1 of cell (i,j), shown in Fig. 20, due to flux entering the left face, is

$$\psi_L(u,v) = \psi_L e^{-\epsilon_y u/\alpha} \quad \text{for } 0 \le u \le \alpha v \ , \qquad (66)$$

where $u = x/\Delta x$ and $v = y/\Delta y$. In the ISC method, particles flow from the bottom of cell $(i-1,j)$ through region 3 of that cell, where they are joined by source particles. Together, these particles flow into and through region 1 of cell (i,j). Thus, Eq. (66) of the SC method is replaced by Eq. (67) for the ISC method:

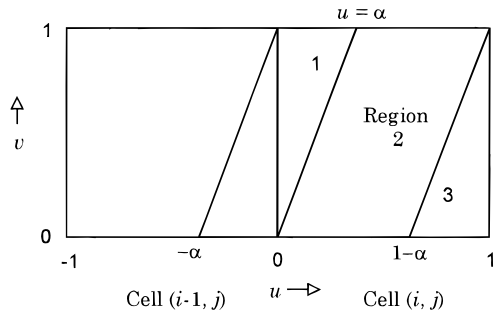

Fig. 20. Cell regions used in deriving independent characteristic methods.

$$\psi_L(u,v) = \psi_{BL}\exp[-\epsilon_y^L(v-u/\alpha)-\epsilon_y u/\alpha] + S_{AL}\frac{\Delta y}{\eta}\int_0^{v-u/\alpha}\exp[-\epsilon_y^L(v-u/\alpha-v') - \epsilon_y u/\alpha]\,dv' \quad . \tag{67}$$

The moments of this flux, over region 1 of cell (i,j), and along that part of the top of cell (i,j) lying on the boundary of region 1, replace the corresponding terms of the SC method. The resulting ISC formulas are

$$\psi_T = \psi_{BL}\alpha e^{-\epsilon_y^L}\mathcal{M}_0(\Delta\epsilon_y) + S_{AL}\frac{\Delta y}{\eta}\alpha\mathcal{M}_0(\epsilon_y^L,\epsilon_y) + \psi_B(1-\alpha)e^{-\epsilon_y} + S_A\frac{\Delta y}{\eta}[\alpha\mathcal{M}_1(\epsilon_y)+(1-\alpha)\mathcal{M}_0(\epsilon_y)] \quad , \tag{68}$$

$$\psi_R = \psi_B\mathcal{M}_0(\epsilon_y) + S_A\frac{\Delta y}{\eta}\mathcal{M}_1(\epsilon_y) \quad , \tag{69}$$

$$\psi_L = \psi_{BL}\mathcal{M}_0(\epsilon_y^L) + S_{AL}\frac{\Delta y}{\eta}\mathcal{M}_1(\epsilon_y^L) \quad , \tag{70}$$

and

$$\psi_A = \psi_{BL}\alpha\mathcal{M}_0(\epsilon_y^L,\epsilon_y) + S_{AL}\frac{\Delta y}{\eta}\alpha\mathcal{M}_1(\epsilon_y^L,\epsilon_y) + \psi_B[(1-\alpha)\mathcal{M}_0(\epsilon_y)+\alpha\mathcal{M}_1(\epsilon_y)] + S_A\frac{\Delta y}{\eta}[(1-\alpha)\mathcal{M}_1(\epsilon_y)+\alpha\mathcal{M}_2(\epsilon_y)] \quad , \tag{71}$$

where $\Delta\epsilon_y = \epsilon_y - \epsilon_y^L$ and the two-dimensional exponential moments functions are defined as

$$\mathcal{M}_n(\epsilon_1,\epsilon_2) = \int_0^1 du(1-u)^n e^{-\epsilon_1 u}\int_0^u dv\, e^{(\epsilon_1-\epsilon_2)v} \quad . \tag{72}$$

Because ψ_R and ψ_L are not used in passing information among the cells during the sweep, they need not be computed. Their formulas are presented because it may be desirable to compute them to obtain currents through surfaces of interest in the transport problem or to check the balance equation for particle conservation.

To interpret these formulas in terms of the foregoing analysis, consider cell (i,j) and its neighbor on the right, cell $(i+1,j)$. In cell (i,j), we have $g_{TB} = (1-\alpha)e^{-\epsilon_y}$, while in cell $(i+1,j)$, we have the equivalent of $g_{TL}g_{RB} = \alpha e^{-\epsilon_y^R}\mathcal{M}_0(\epsilon_y^R - \epsilon_y)$. Thus, for the ISC method,

$$a = (1-\alpha)e^{-\epsilon_y} + \alpha e^{-\epsilon_y^R}\mathcal{M}_0(\epsilon_y^R - \epsilon_y) \tag{73}$$

and

$$\tau_{eff} = \tau\,\frac{(1-\alpha)e^{-\epsilon_y} + \alpha e^{-\epsilon_y^R}\mathcal{M}_0(\epsilon_y^R-\epsilon_y)}{e^{-\epsilon_y^R}\mathcal{M}_0(\epsilon_y^R-\epsilon_y)} \quad . \tag{74}$$

Because $\mathcal{M}_0(0) = 1$, these reduce to $a = e^{-\epsilon_y} = a_{exact}$ and $\tau_{eff} = \tau$ if both cells have the same cross section. Thus, the ray propagation by the ISC method for the example is exact (in this sense) and has already been presented as Fig. 2. What remains to be done is to test the performance of the method for transport problems that include emission sources and scattering.

A few final points of implementation remain. Cells on the left boundary of the mesh do not have a neighbor to the left. With a reflection boundary condition, of course, the cell (as reflected) is its own neighbor to the left. A vacuum boundary with a specified incident flux could be treated using the SC equations for that cell. Alternatively, a column of phantom cells can be placed outside the mesh of real cells, with ψ_{BL} equaling the specified incident flux and $\sigma_L = 0$ (i.e., vacuum phantom cells). Then, the ISC equations apply to the leftmost real cell, retaining the opportunity for simple data parallelism. This is the approach shown in algorithm 3 (Appendix D). Quadrature directions that project exactly along the cell diagonal ($\tau = \tau_d$) can be included in either the upward sweep or the rightward sweep. Either choice introduces some asymmetry into the solution of an exchange-symmetric ($x \leftrightarrow y$) problem. This could be avoided by including such directions in both sweeps, with halved weights, or by choosing quadrature sets that do not include such directions. Alternatively, the smallness of the effect of this asymmetry could be used as a measure of performance for a given problem.

IV.B. Independent Linear Characteristic Method

The ILC method bears the same relation to LC as ISC does to SC. The derivation follows the same lines, differing only by expanding the fluxes and sources using first moments as well as zeroth moments. The ILC formulas consist of the LC formulas in Appendix C with replacements for the contributions from the flux entering

through the left face. The replacement formulas are presented in Appendix E.

The inclusion of first moments results in considerably greater complexity, including the need for the evaluation of multidimensional exponential moments functions, defined as

$$\mathcal{M}_n(\epsilon_1,\ldots,\epsilon_k) \equiv \int_0^1 dt_1(1-t_1)^n e^{-\epsilon_1 t_1} \times \int_0^{t_1} dt_2\, e^{(\epsilon_1-\epsilon_2)t_2} \cdots \int_0^{t_{k-1}} dt_k\, e^{(\epsilon_{k-1}-\epsilon_k)t_k} \quad . \tag{75}$$

In particular, exponential moments functions with repeated arguments arise because integrals of the following form are required when first moments are included. These integrals are reduced to such exponential moments functions as follows:

$$\begin{aligned}\int_0^1 du(1-u)^n e^{-\epsilon_y^L} \int_0^u dv\, v^k e^{(\epsilon_y^L-\epsilon_y)v} &= k! \int_0^1 du(1-u)^n e^{-\epsilon_y^L} \int_0^u dv\, e^{(\epsilon_y^L-\epsilon_y)v} \\ &\quad \times \int_0^v dt_1\, e^{(\epsilon_y-\epsilon_y)t_1} \cdots \int_0^{t_{k-1}} dt_k\, e^{(\epsilon_y-\epsilon_y)t_k} \\ &= k!\mathcal{M}_n(\epsilon_y^L,\epsilon_y,\ldots,\epsilon_y) \quad ,\end{aligned} \tag{76}$$

where ϵ_y appears $k+1$ times in the argument list.

Numerically well-conditioned algorithms for evaluation of some of these multidimensional exponential moments functions have been presented previously.[9] Algorithms for the rest can be developed along similar lines. If the optical thickness of the cells is restricted to a range in which the method works well, such as $0 \le \epsilon_y \le 2$, then execution speed could be optimized by using series expansions to simplify the formulas to matrix or tensor reductions (dot products), thus taking advantage of the hardware optimizations for linear algebra that are common among modern processors.

The performance of the ILC method is demonstrated by Fig. 21. The method has the same outstanding beam quality as the LC method, but the attenuation and direction of propagation are exact (to 15 digits).

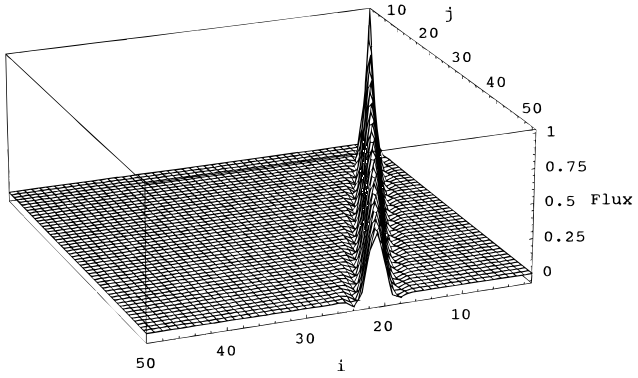

Fig. 21. The ILC method.

V. IMPLICATIONS FOR MASSIVE PARALLELISM

In two dimensions, the ISC and ILC methods allow all the cells in a row of the spatial mesh to be computed in parallel. Algorithm 3 (Appendix D) shows one way in which this can be done. In fact, any characteristic-like method could be implemented with this row parallelism. For the directions analyzed here, cell (i,j) would receive some of the inputs for cell $(i-1,j)$ and would use those to calculate the moments of the flux passing between the two cells. That would then be used in the usual way to compute the flux moments within and leaving cell (i,j). For a direction up and to the right, but below the cell diagonal, cell (i,j) would receive some of the inputs for cell $(i,j-1)$. However, the independent methods developed here go one step further. To provide more accurate propagation, they calculate the flux moments within and leaving cell (i,j) directly from the input data for both cells, thus eliminating the intermediate approximation of the flux along the boundary between the two cells. Algorithm 3 (Appendix D) also provides independence of the sweeps for different ordinates by hoisting the boundary condition calculations above the transport loop. This provides an opportunity for domain decomposition in angle as well as space.

Schemes that are not characteristic-like cannot be implemented with row parallelism, although they can use diagonal parallelism, as follows. For an up-to-the-right direction, the sweep could proceed with diagonally adjacent cells executed in parallel: Cell (1,1) is followed by both cells (1,2) and (2,1); these are followed by (1,3), (2,2), and (3,1), and so forth. Unfortunately, diagonal parallelism is more complicated to program and less efficient to execute than row parallelism. With an $n \times n$ mesh, n processors can be used either way. However, with row parallelism they are fully occupied, whereas with diagonal parallelism one-half of them will be idle, on average. (Overlapping one angular sweep with another can reduce the idle fraction, at the cost of further complexity.)

Independent methods can achieve even more impressive parallelism in three-dimensional problems, using plane parallelism: Whole planes of cells can be executed in parallel. Thus, with an $n \times n \times n$ mesh, n^2 processors can be fully occupied. Furthermore, by distributing the flux arrays using domain decomposition into blocks in

each of the three dimensions (HPF's BLOCK, BLOCK, BLOCK distribution), and overlapping the sweeps for different angular quadrature directions, k^3 processors (where k divides n and k is less than or on the order of one sixth of the number of quadrature directions) could be kept nearly fully occupied.

Of course, the optimal parallel implementation will be dependent on machine-specific features, such as cache line numbers and sizes, latency periods for memory and interprocessor or intercache communications, and the handling of memory contention. Nevertheless, the opportunity to turn the innermost DO loop(s) into DO INDEPENDENT loop(s), as shown in algorithm 3 (Appendix D), should always be advantageous.

VI. SUMMARY AND CONCLUSIONS

A good spatial quadrature method should have a sound mathematical basis.[a] It should transport particles that enter the mesh through a single cell boundary or that leave a source cell through a single face in rays that propagate across the mesh in the intended directions $\hat{\Omega}_n$ and that are accurately attenuated by collisions. Each ray should be a well-collimated symmetric smooth beam, preferably with positive flux values, or with only narrow, small, rapidly damped oscillations located symmetrically along its edges. Table I summarizes the performance of the methods tested.

The testing here has examined only cell-edge fluxes because those are the fluxes that propagate across the mesh as rays and pass currents between regions. Any method that enforces the particle conservation (balance equations) within every cell and that provides accurate cell-edge fluxes must provide accurate cell-average fluxes. We consider such a method to be reliable. If the cell-edge fluxes are inaccurate or nonsensical, it is possible for the cell-average fluxes to be accurate, but there is no assurance of this. Therefore, we consider methods that produce inaccurate or nonsensical cell-edge fluxes to be unreliable.

Among the methods tested, ISC, ILC, and LC were the best performers. ISC and ILC provide exact attenuation and direction of propagation and provide independent calculations for laterally adjacent cells. This independence supports row-parallel (in two dimensions) or plane-parallel (in three dimensions) implementation in vector or parallel computers. The LC method, being a characteristic method, can also be implemented to provide adjacent cell independence, and the good performance and convergence properties of LC are well known.

With regard to ray propagation, the trade-off between ISC and ILC is between positivity and lesser computational cost per cell (ISC) and tighter collimation at higher computational cost per cell (ILC). However, once scattering sources are included in the transport problem, ILC will have the advantage of much more accurate representation of the scattering source distribution within each cell so that coarser meshes can be used, offsetting the computational cost per cell and reducing memory requirements.

The DD methods fail nearly all these criteria. Without fixups to ensure positivity, or where they are not actually invoked, DD solutions are the superposition of rays that are entirely unphysical. The lateral oscillations are undamped relative to the intended ray. They form a ray of peak oscillations that actually propagates in a direction that is the reflection of the intended direction across the cell diagonal. This unphysical ray is not visibly attenuated as it propagates through the mesh. Note that in many problems, especially those that are nearly diffusive, rays do not propagate far through the mesh, and the flux is only slightly anisotropic (even if the scattering is highly anisotropic). Combine this with sources that are smoothly distributed, resulting in approximate destructive interference of adjacent rays of oscillations, and DD can give reasonably accurate results for global quantities. It should be no surprise, however, that unphysical artifacts of its unphysical propagation of particles through the mesh should arise in many problems.

The DD method has a sound mathematical basis as a divided difference approximation to the transport equation. If it were unstable, causing overflow errors, it would have been recognized as unsatisfactory long ago. However, it is only unstable in a relative sense: the lateral oscillations grow without bound relative to the attenuating correct ray.

Fixups that ameliorate the symptoms of this behavior, such as theta-weighted DD, are, in the opinion of this author, ad hoc and dangerous. To the extent that they strive for DD weights where no fixup is needed, they provide a superposition of unphysical representations of rays, and the superposition of nonsense is still nonsense, even if it is sometimes accurate. To the extent that they adjust the weights to stabilize the method, they lack a sound mathematical basis.

The LL nodal method has a sound mathematical basis and provides excellent accuracy but poor beam quality. The LN method is contaminated by the DD approximation used to uncouple the LL equations, resulting in acceptable computational cost but undamped lateral oscillations. Fixups are nonlinear, ad hoc, destroy first-moment conservation, and degrade accuracy, although they do, at the least, improve the quality of an isolated beam.

[a] In 1983, as a graduate student, I presented an idea for reducing ray effects to, among others, K. Lathrop. He replied that it was an ingenious idea and might work out but that it had no mathematical foundation. Therefore, if it failed, I would not know why, so I would have no starting point for fixing it. Whereas, if it seemed to help, I would not know how and why, so how would I find confidence in its reliability? Furthermore, how would I improve it?

TABLE I

Performance Summary

Method	τ^{eff}	$(a/a_{exact}) - 1$ (at row 50)	Linear	Positive	Accuracy	Lateral Oscillations
Exact	2.48239	0				
SC	2.44	+73%	✓	✓	Poor	None
Step	3.9	373	✓	✓	Very poor	None
DD	*	*	✓		*	One-sided, severely undamped
DZ	1.5 to 2.1	−57%		✓	Very poor	None
LL	2.483	+0.004%	✓		Excellent	One-sided, moderate size, moderately damped
LLF	2.1 to 2.467	+4.0%		✓	Fair	None
LN	2.428	+1.3%			*	One-sided, undamped (ringing dominates ray)
LNF	2.35 to 2.40	+6.0%		✓	Fair	One-sided, small, moderately damped
LD	2.46	−6.5%	✓		Fair	One-sided, large, moderately well-damped
BLD	2.46	−6.5%	✓		Fair	Approximately symmetric, small, strongly damped
LC	2.4813 to 2.482	−0.31%	✓		Good	Approximately symmetric, small, strongly damped
LCF	2.30 to 2.477	−0.31%		✓	Fair	None
Approximate LC	2.46	−0.66%	✓		Not as good as LC	Asymmetric, larger than LC, strongly damped
Approximate LCF	2.30 to 2.44	−0.68%		✓	Fair	None
ISC	$= \tau - 10^{-15}$	$\pm 5 \times 10^{-15}$	✓	✓	Exact	None
ILC	$= \tau - 10^{-15}$	$\pm 5 \times 10^{-15}$	✓		Exact	Approximately symmetric, small, strongly damped

*Not meaningful (due to lateral oscillations).

The LD method, as a finite element method, has a sound mathematical basis and combines moderate accuracy, moderate beam quality, and moderate computational cost per cell. The BLD method shares the mathematical basis, retains the moderate accuracy, and improves beam quality at an increase in cost.

VII. RECOMMENDATIONS

The DD method is inexpensive but unphysical in ways that should induce us to abandon it and all its offspring. The LL method has good accuracy and fair beam quality, but as implemented (as the LN method), the beam quality is ruined by a DD approximation to obtain uncoupled LN equations that are less expensive in cost per cell. The LD method is another approximation to LL, in which a step approximation is used in the first moments and a Padé approximation is used in place of an exponential. The result is degraded beam quality and degraded accuracy at decreased computational cost per cell. The LD method has been in use for at least 25 yr (Ref. 14). The BLD method increases cost, requiring a linear system of four equations to be solved in each cell for each direction. It improves beam quality but not attenuation accuracy and has good thick-cell diffusion performance. Perhaps BLD should be more widely used. The LC method is a fine algorithm that has been available for 15 yr but is not widely used, perhaps partly because of the approximation of the first moments by chords to reduce computational cost by 20% while destroying first-moment conservation.

As central processors increase in speed, main memory access becomes more limiting, while arithmetic becomes less so. As we move to parallel machines, interprocessor or intercache communications tend to be the limit on speed. In response to these changes, algorithm and code design decisions should be based on the precept of implementing mathematically sound methods with full fidelity rather than introducing approximations that decrease arithmetic cost per cell while degrading performance.

The LC method, using the equations in Appendix C together with robust routines for the exponential moments functions, is a step in this direction. The ILC method, using the additional equations in Appendix E, is perhaps another such step. The ILC method may (or may not) prove to be a worthwhile modification of the LC method when applied to realistic transport problems. The author intends to report on this after implementing the method on a parallel machine.

APPENDIX A

ALGORITHM 1: DISCRETE ORDINATES MESH SWEEP

```
Do n=1,nMax
   If (mu(n)>0 .and. eta(n)>0) then ! Quadrant 1
      DO INDEPENDENT j=1,jMax
         ! apply b.c. on left edge
         !for example, symmetry boundary
         nn = [index of direction with mu(nn)=-mu(n)]
         fRight(0,j,n) = fRight(0,j,nn)
      End do
      DO INDEPENDENT i=1,iMax
         ! apply b.c. on bottom boundary
         ! for example, symmetry boundary
         nn = [index of direction with eta(nn) = −eta(n)]
         fTop(i,0,n) = fTop(i,0,nn)
      End do
      Do j=1,jMax
         Do i=1,iMax
            Call SQ(fTop(i-1,j,n),fRight(i,j-1,n),&
                    fAve(i,j,n),fTop(i,j,n),fRight(i,j,n),&
                    [other parameters])
         End do
      End do
   Else if . . . ! Other quadrants [4 total]
      . . .
   End if
End do
```

```
Subroutine SQ(fBottom, fLeft, fAve, fTop, fRight,&
               [other parameters])
   ! fBottom and fLeft are entering fluxes, input
   ! fAve, fTop, and fRight are result fluxes
   ! [other parameters] include cross section, source,
   ! cell dimensions, mu(n) and eta(n)
```

APPENDIX B

ALGORITHM 2: MESH SWEEP FOR CHARACTERISTIC-LIKE METHOD

```
Do n=1,nMax
   If (mu(n)>0.and.eta(n)>0.and.eta(n)>=mu(n)*tanDiag(n)) then
      ! Above diagonal in quadrant 1
      DO INDEPENDENT j=1,jMax
         ! apply b.c. on left edge
         !for example, symmetry boundary
         nn = [index of direction with mu(nn)=-mu(n)]
         fRight(0,j,n) = fRight(0,j,nn)
      End do
      DO INDEPENDENT i=1,iMax
         ! apply b.c. on bottom boundary
         ! for example, symmetry boundary
         nn = [index of direction with eta(nn) = −eta(n)]
         fTop(i,0,n) = fTop(i,0,nn)
      End do
      Do j=1,jMax ! note data dependencies
         Do i=1,iMax ! note data dependencies
            Call CLSQ(fTop(i-1,j,n),fRight(i,j-1,n),&
                      fAve(i,j,n),fTop(i,j,n),fRight(i,j,n),&
                      mu(n),eta(n),dx,dy,[other parameters])
         End do
      End do
   Else if (mu(n)>0.and.eta(n)>0.and.eta(n)<mu(n)*tanDiag(n)) then
      ! Below diagonal in quadrant 1
      DO INDEPENDENT j=1,jMax
         fRight(0,j,n) = . . . ! apply b.c. on left edge
      End do
      DO INDEPENDENT i=1,iMax
         fTop(i,0,n) = . . . ! apply b.c. on bottom edge
      End do
      Do j=1,jMax ! note data dependencies
         Do i=1,iMax ! note data dependencies
            Call CLSQ(fRight(i,j-1,n),fTop(i-1,j,n),&
                      fAve(i,j,n),fRight(i,j,n),fTop(i,j,n),&
                      eta(n),mu(n),dy,dx,[other parameters])
         End do
      End do
   Else if . . . ! Other orientations [8 total]
      . . .
   End if
End do

Subroutine CLSQ(fBottom, fLeft, fAve, fTop, fRight,&
                  mu, eta, dx, dy, [other parameters])
```

```
! fBottom and fLeft are entering fluxes, input
! fAve, fTop, and fRight are result fluxes,
! mu and eta are such that flux crosses cell
! from bottom to top, from bottom to right,
! and from left to top, but not from left to right,
! dx is width of cell along bottom and top edges,
! dy is width of cell along left and right edges,
! [other parameters] include cross section, source.
```

APPENDIX C

FORMULAS FOR THE LINEAR CHARACTERISTIC METHOD

The formulas for the LC method are obtained as described in Sec. III.C.1. They have been derived here by manipulating the integrals of the closed-form solution that define the flux moments over the cell and over its outflow edges in order to express them directly in terms of exponential moments functions. The notation for the flux moments indicates which moment is being taken, over which region of the cell, and the source of the particles. In each case, the streaming direction is presumed to be such that particles enter the cell through the bottom and left edges and exit through the right and top edges. Particles that enter through the left edge and do not collide flow out through the top edge only, as for the example ray in this paper.

The contributions of the flux entering through the left face are as follows:

$$\psi_{TL} = \psi_L \alpha \mathcal{M}_0(\epsilon_y) + \theta_L \alpha [2\mathcal{M}_1(\epsilon_y) - \mathcal{M}_0(\epsilon_y)] \ , \tag{C.1}$$

$$\theta_{TL} = \psi_L 3\alpha [(2\alpha - 1)\mathcal{M}_0(\epsilon_y) - 2\alpha \mathcal{M}_1(\epsilon_y)] + \theta_L [(1 - 2\alpha)\mathcal{M}_0(\epsilon_y) + (6\alpha - 2)\mathcal{M}_1(\epsilon_y) - 4\alpha \mathcal{M}_2(\epsilon_y)] \ , \tag{C.2}$$

$$\psi_{AL} = \psi_L \alpha \mathcal{M}_1(\epsilon_y) + \theta_L \alpha [\mathcal{M}_2(\epsilon_y) - \mathcal{M}_1(\epsilon_y)] \ , \tag{C.3}$$

$$\psi_{XL} = \psi_L 3\alpha [(2\alpha - 1)\mathcal{M}_1(\epsilon_y) - 2\alpha \mathcal{M}_2(\epsilon_y)] + \theta_L 3\alpha [(1 - 2\alpha)\mathcal{M}_1(\epsilon_y) + (4\alpha - 1)\mathcal{M}_2(\epsilon_y) - 2\alpha \mathcal{M}_3(\epsilon_y)] \ , \tag{C.4}$$

and

$$\psi_{YL} = \psi_L 3\alpha [\mathcal{M}_1(\epsilon_y) - \mathcal{M}_2(\epsilon_y)] + \theta_L \alpha [-3\mathcal{M}_1(\epsilon_y) + 6\mathcal{M}_2(\epsilon_y) - 2\mathcal{M}_3(\epsilon_y)] \ . \tag{C.5}$$

The contributions of the flux entering through the bottom face are as follows:

$$\psi_{TB} = \psi_B (1 - \alpha) \exp(-\epsilon_y) - \theta_B \alpha (1 - \alpha) \exp(-\epsilon_y) \ , \tag{C.6}$$

$$\theta_{TB} = \psi_B 3\alpha (1 - \alpha) \exp(-\epsilon_y) + \theta_B (1 - 3\alpha + 2\alpha^3) \exp(-\epsilon_y) \ , \tag{C.7}$$

$$\psi_{RB} = \psi_B \mathcal{M}_0(\epsilon_y) + \theta_b [(1 - 2\alpha)\mathcal{M}_0(\epsilon_y) + 2\alpha \mathcal{M}_1(\epsilon_y)] \ , \tag{C.8}$$

$$\theta_{RB} = \psi_B 3[\mathcal{M}_0(\epsilon_y) - 2\mathcal{M}_1(\epsilon_y)] + \theta_B 3[(1 - 2\alpha)\mathcal{M}_0(\epsilon_y) + (6\alpha - 2)\mathcal{M}_1(\epsilon_y) - 4\alpha \mathcal{M}_2(\epsilon_y)] \ , \tag{C.9}$$

$$\psi_{AB} = \psi_B [(1 - \alpha)\mathcal{M}_0(\epsilon_y) + \alpha \mathcal{M}_1(\epsilon_y)] + \theta_B \alpha [-(1 - \alpha)\mathcal{M}_0(\epsilon_y) + (1 - 2\alpha)\mathcal{M}_1(\epsilon_y) + \alpha \mathcal{M}_2(\epsilon_y)] \ , \tag{C.10}$$

$$\begin{aligned} \psi_{XB} = {} & \psi_B 3\alpha [(1 - \alpha)\mathcal{M}_0(\epsilon_y) + (2\alpha - 1)\mathcal{M}_1(\epsilon_y) - \alpha \mathcal{M}_2(\epsilon_y)] \\ & + \theta_B [(1 - 3\alpha + 2\alpha^3)\mathcal{M}_0(\epsilon_y) + (3\alpha - 6\alpha^3)\mathcal{M}_1(\epsilon_y) + 6\alpha^3 \mathcal{M}_2(\epsilon_y) - 2\alpha^3 \mathcal{M}_3(\epsilon_y)] \ , \end{aligned} \tag{C.11}$$

and

$$\begin{aligned} \psi_{YB} = {} & \psi_B 3[(1 - \alpha)\mathcal{M}_0(\epsilon_y) + (3\alpha - 2)\mathcal{M}_1(\epsilon_y) - 2\alpha \mathcal{M}_2(\epsilon_y)] \\ & + \theta_B 3\alpha [(\alpha - 1)\mathcal{M}_0(\epsilon_y) + (3 - 4\alpha)\mathcal{M}_1(\epsilon_y) + (5\alpha - 2)\mathcal{M}_2(\epsilon_y) - 2\alpha \mathcal{M}_3(\epsilon_y)] \ . \end{aligned} \tag{C.12}$$

Finally, the moments of the flux due to the source within the cell are as follows:

$$\psi_{TS} = q_A[(1-\alpha)\mathcal{M}_0(\epsilon_y) + \alpha\mathcal{M}_1(\epsilon_y)] + q_X\alpha[-(1-\alpha)\mathcal{M}_0(\epsilon_y) - 2\alpha\mathcal{M}_1(\epsilon_y) + \alpha\mathcal{M}_2(\epsilon_y)]$$
$$+ q_Y[-(1-\alpha)\mathcal{M}_0(\epsilon_y) + (2-3\alpha)\mathcal{M}_1(\epsilon_y) + 2\alpha\mathcal{M}_2(\epsilon_y)] \ , \tag{C.13}$$

$$\theta_{TS} = q_A 3\alpha[(1-\alpha)\mathcal{M}_0(\epsilon_y) + (2\alpha-1)\mathcal{M}_1(\epsilon_y) - \alpha\mathcal{M}_2(\epsilon_y)]$$
$$+ q_X[(1-3\alpha-2\alpha^3)\mathcal{M}_0(\epsilon_y) + (3\alpha-6\alpha^3)\mathcal{M}_1(\epsilon_y) + 6\alpha^3\mathcal{M}_2(\epsilon_y) - 2\alpha^3\mathcal{M}_3(\epsilon_y)]$$
$$+ q_Y 3\alpha[-(1-\alpha)\mathcal{M}_0(\epsilon_y) + (3-4\alpha)\mathcal{M}_1(\epsilon_y) + (5\alpha-2)\mathcal{M}_2(\epsilon_y) - 2\alpha\mathcal{M}_3(\epsilon_y)] \ , \tag{C.14}$$

$$\psi_{RS} = q_A\mathcal{M}_1(\epsilon_y) + q_X[(1-2\alpha)\mathcal{M}_1(\epsilon_y) + 2\alpha\mathcal{M}_2(\epsilon_y)] + q_Y[\mathcal{M}_2(\epsilon_y) - \mathcal{M}_1(\epsilon_y)] \ , \tag{C.15}$$

$$\theta_{RS} = q_A 3[\mathcal{M}_1(\epsilon_y) - \mathcal{M}_2(\epsilon_y)] + q_X 3[(1-2\alpha)\mathcal{M}_1(\epsilon_y) + (4\alpha-1)\mathcal{M}_2(\epsilon_y) - 2\alpha\mathcal{M}_3(\epsilon_y)]$$
$$+ q_Y[-3\mathcal{M}_1(\epsilon_y) + 6\mathcal{M}_2(\epsilon_y) - 2\mathcal{M}_3(\epsilon_y)] \ , \tag{C.16}$$

$$\psi_{AS} = q_A[(1-\alpha)\mathcal{M}_1(\epsilon_y) - \alpha\mathcal{M}_2(\epsilon_y)] + (q_X\alpha + q_Y)[-(1-\alpha)\mathcal{M}_1(\epsilon_y) + (1-2\alpha)\mathcal{M}_2(\epsilon_y) + \alpha\mathcal{M}_3(\epsilon_y)] \ , \tag{C.17}$$

$$\psi_{XS} = q_A 3\alpha[(1-\alpha)\mathcal{M}_1(\epsilon_y) + (2\alpha-1)\mathcal{M}_2(\epsilon_y) - \alpha\mathcal{M}_3(\epsilon_y)]$$
$$+ q_X[(1-3\alpha+2\alpha^3)\mathcal{M}_1(\epsilon_y) + (3\alpha-6\alpha^3)\mathcal{M}_2(\epsilon_y) + 6\alpha^3\mathcal{M}_3(\epsilon_y) - 2\alpha^3\mathcal{M}_4(\epsilon_y)]$$
$$+ q_Y 3\alpha[-(1-\alpha)\mathcal{M}_1(\epsilon_y) + (2-3\alpha)\mathcal{M}_2(\epsilon_y) + (3\alpha-1)\mathcal{M}_3(\epsilon_y) - \alpha\mathcal{M}_4(\epsilon_y)] \ , \tag{C.18}$$

and

$$\psi_{YS} = q_A 3[(1-\alpha)\mathcal{M}_1(\epsilon_y) + (2\alpha-1)\mathcal{M}_2(\epsilon_y) - \alpha\mathcal{M}_3(\epsilon_y)]$$
$$+ q_X 3\alpha[-(1-\alpha)\mathcal{M}_1(\epsilon_y) + (2-3\alpha)\mathcal{M}_2(\epsilon_y) + (3\alpha-1)\mathcal{M}_3(\epsilon_y) - \alpha\mathcal{M}_4(\epsilon_y)]$$
$$+ q_Y[-3(1-\alpha)\mathcal{M}_1(\epsilon_y) + (6-9\alpha)\mathcal{M}_2(\epsilon_y) + (8\alpha-2)\mathcal{M}_3(\epsilon_y) - 2\alpha\mathcal{M}_4(\epsilon_y)] \ , \tag{C.19}$$

where

$$q_A = S_A \frac{\Delta y}{\eta} \ , \tag{C.20}$$

$$q_X = S_X \frac{\Delta y}{\eta} \ , \tag{C.21}$$

and

$$q_Y = S_Y \frac{\Delta y}{\eta} \ . \tag{C.22}$$

APPENDIX D

ALGORITHM 3: MESH SWEEP FOR INDEPENDENT CHARACTERISTIC-LIKE METHOD

```
! Handle boundary conditions on all boundaries in first loop
! This eliminates data dependencies among rays in second loop
DO INDEPENDENT n=1,nMax ! Angular domain decomposition
   If (mu(n)>0.and.eta(n)>0.and.eta(n)>=mu(n)*tanDiag(n)) then
      ! Above diagonal in quadrant 1
```

```
      DO INDEPENDENT i=1,iMax ! row-parallel
         ! apply b.c. on bottom boundary
         ! for example, symmetry boundary
         nn = [index of direction with eta(nn) = −eta(n)]
         fTop(i,0,n) = fTop(i,0,nn)
      End do
      DO INDEPENDENT j=1,jMax ! column-parallel
         ! apply b.c. on left to fill phantom column i=0
         ! for example, symmetry boundary
         nn = [index of direction with mu(nn)=-mu(n)]
         fTop(0,j,n) = fTop(1,j,nn)
         source(0,j,n) = source(1,j,nn)
      End do
   Else if (mu(n)>0.and.eta(n)>0.and.eta(n)<mu(n)*tanDiag(n)) then
      ! Below diagonal in quadrant 1
      DO INDEPENDENT j=1,jMax ! column-parallel
         ! for example, symmetry boundary
         nn = [index of direction with mu(nn)=-mu(n)]
         fRight(0,j,n) = fRight(0,j,nn)
      End do
      DO INDEPENDENT i=1,iMax ! row-parallel
         ! apply b.c. on bottom to fill phantom row j=0
         ! for example, symmetry boundary
         nn = [index of direction with eta(nn) = −eta(n)]
         fTop(i,0,n) = fTop(i,1,nn)
         source(i,0,n) = source(i,0,nn)
      End do
   Else if . . . ! other orientations [8 total]
      . . .
   End if
End do
! Transport through cells, a row or column at a time
DO INDEPENDENT n=1,nMax ! Angular domain decomposition
   If (mu(n)>0.and.eta(n)>0.and.eta(n)>=mu(n)*tanDiag(n)) then
      ! Above diagonal in quadrant 1
      Do j=1,jMax ! note data dependency in j but not i
         DO INDEPENDENT i=1,iMax ! row-parallel
            Call ICLSQ(fTop(i-1,j-1,n),fTop(i,j-1,n),&
                       fAve(i,j,n),fTop(i,j,n),fRight(i,j,n),&
                       mu(n),eta(n),dx,dy,&
                       source(i-1,j,n),source(i,j,n),&
                       [other parameters])
         End do
      End do
   Else if (mu(n)>0.and.eta(n)>0.and.eta(n)<mu(n)*tanDiag(n)) then
      ! Below diagonal in quadrant 1
      Do i=1,iMax ! note data dependency in i but not j
         DO INDEPENDENT j=1,jMax ! column-parallel
            Call ICLSQ(fRight(i-1,j-1,n),fRight(i-1,j,n),&
                       fAve(i,j,n),fRight(i,j,n),fTop(i,j,n),&
                       eta(n),mu(n),dy,dx,&
                       source(i,j-1,n), source(i,j,n),&
                       [other parameters])
         End do
      End do
   Else if . . . ! other orientations [8 total]
      . . .
```

```
   End if
End do

Subroutine ICLSQ(fBottomLeft, fBottom,&
                 fAve, fTop, fRight,&
                 mu, eta, dx, dy, &
                 sourceLeft, source, [other parameters])
   ! fBottomLeft is flux entering bottom
   ! of cell to the left
   ! sourceLeft is source in cell to left
   ! fLeft is flux entering bottom of cell
   ! source is source in the cell
   ! fAve, fTop, and fRight are result fluxes
   ! fRight is not used to couple cells, only output
   ! to determine currents between regions, etc.
   ! mu and eta are such that flux crosses cell
   ! from bottomLeft to top, from bottom to top,
   ! from bottom to right, and from left to top,
   ! but not from bottomLeft to right.
   ! dx is width of cell along bottom and top edges,
   ! dy is width of cell along left and right edges,
   ! [other parameters] include cross section.
```

APPENDIX E

REPLACEMENT FORMULAS FOR THE INDEPENDENT LINEAR CHARACTERISTIC METHOD

The ILC method differs from the LC method only in the treatment of the flux that flows into the cell from the laterally upstream cell, as described earlier. Thus, the formulas in this appendix replace formulas (C.1) through (C.5) of Appendix C. This flux has two components: that due to inflow into the neighboring cell and that due to any source in the neighboring cell. These are presented as the contributions due to ψ_{BL} and θ_{BL}, the moments of the flux entering the bottom face of the cell to the left, and due to S_{AL}, S_{XL}, and S_{YL}, the moments of the source in the cell to the left. Note that in this appendix, a subscript or superscript L refers to the cell to the left, that is, cell $(i-1,j)$, whereas in Appendix C, it refers to the left face of the cell being computed, that is, cell (i,j).

The formulas for the contribution of the flux due to ψ^{BL} and θ_{BL} are as follows:

$$\psi_{TBL} = \psi_{BL}\alpha\exp(-\epsilon_y^L)\mathcal{M}_0(\Delta\epsilon_y) + \theta_{BL}\alpha\exp(-\epsilon_y^L)[\mathcal{M}_0(\Delta\epsilon_y) - 2\alpha\mathcal{M}_1(\Delta\epsilon_y)] \ , \tag{E.1}$$

$$\begin{aligned}\theta_{TBL} = {} & \psi_{BL}3\alpha\exp(-\epsilon_y^L)[(2\alpha-1)\mathcal{M}_0(\Delta\epsilon_y) - 2\alpha\mathcal{M}_1(\Delta\epsilon_y)] + \theta_{BL}3\alpha\exp(-\epsilon_y^L) \\ & \times[(2\alpha-1)\mathcal{M}_0(\Delta\epsilon_y) - 4\alpha^2\mathcal{M}_1(\Delta\epsilon_y) + 4\alpha^2\mathcal{M}_2(\Delta\epsilon_y)] \ ,\end{aligned} \tag{E.2}$$

$$\psi_{ABL} = \psi_{BL}\alpha\mathcal{M}_0(\epsilon_y^L,\epsilon_y) + \theta_{BL}\alpha[(1-2\alpha)\mathcal{M}_0(\epsilon_y^L,\epsilon_y) + 2\alpha\mathcal{M}_1(\epsilon_y^L,\epsilon_y) + 2\alpha\mathcal{M}_0(\epsilon_y^L,\epsilon_y,\epsilon_y)] \ , \tag{E.3}$$

$$\begin{aligned}\psi_{XBL} = {} & \psi_{BL}3\alpha[2\alpha\mathcal{M}_0(\epsilon_y^L,\epsilon_y,\epsilon_y) - \mathcal{M}_0(\epsilon_y^L,\epsilon_y)] \\ & + \theta_{BL}3\alpha[(2\alpha-1)\mathcal{M}_0(\epsilon_y^L,\epsilon_y) - 2\alpha\mathcal{M}_1(\epsilon_y^L,\epsilon_y) - 4\alpha^2\mathcal{M}_0(\epsilon_y^L,\epsilon_y,\epsilon_y) + 4\alpha^2\mathcal{M}_1(\epsilon_y^L,\epsilon_y,\epsilon_y) \\ & \quad + 8\alpha^2\mathcal{M}_0(\epsilon_y^L,\epsilon_y,\epsilon_y,\epsilon_y)] \ ,\end{aligned} \tag{E.4}$$

and

$$\begin{aligned}\psi_{YBL} = {} & \psi_{BL}3\alpha[\mathcal{M}_0(\epsilon_y^L,\epsilon_y) - 2\mathcal{M}_1(\epsilon_y^L,\epsilon_y)] \\ & + \theta_{BL}3\alpha[(1-2\alpha)\mathcal{M}_0(\epsilon_y^L,\epsilon_y) + (6\alpha-2)\mathcal{M}_1(\epsilon_y^L,\epsilon_y) - 4\alpha\mathcal{M}_2(\epsilon_y^L,\epsilon_y) + 2\alpha\mathcal{M}_0(\epsilon_y^L,\epsilon_y,\epsilon_y) \\ & \quad - 4\alpha\mathcal{M}_1(\epsilon_y^L,\epsilon_y,\epsilon_y)] \ ,\end{aligned} \tag{E.5}$$

where

$$\Delta\epsilon_y = \epsilon_y - \epsilon_y^L \ . \tag{E.6}$$

The formulas for the contribution of the flux due to S_{AL}, S_{XL}, and S_{YL} are as follows:

$$\begin{aligned}\psi_{TSL} &= q_A^L \alpha \mathcal{M}_0(\epsilon_y^L,\epsilon_y) + q_X^L \alpha[(1-2\alpha)\mathcal{M}_0(\epsilon_y^L,\epsilon_y) + 2\alpha\mathcal{M}_1(\epsilon_y^L,\epsilon_y) + 2\alpha\mathcal{M}_0(\epsilon_y^L,\epsilon_y,\epsilon_y)] \\ &\quad + q_Y^L \alpha[2\mathcal{M}_1(\epsilon_y^L,\epsilon_y) - \mathcal{M}_0(\epsilon_y^L,\epsilon_y)] \ , \end{aligned} \tag{E.7}$$

$$\begin{aligned}\theta_{TSL} &= q_A^L 3\alpha[2\alpha\mathcal{M}_0(\epsilon_y^L,\epsilon_y,\epsilon_y) - \mathcal{M}_0(\epsilon_y^L,\epsilon_y)] \\ &\quad + q_X^L 3\alpha[(2\alpha-1)\mathcal{M}_0(\epsilon_y^L,\epsilon_y) - 2\alpha\mathcal{M}_1(\epsilon_y^L,\epsilon_y) - 4\alpha^2\mathcal{M}_0(\epsilon_y^L,\epsilon_y,\epsilon_y) \\ &\qquad + 4\alpha^2\mathcal{M}_1(\epsilon_y^L,\epsilon_y,\epsilon_y) + 8\alpha^2\mathcal{M}_0(\epsilon_y^L,\epsilon_y,\epsilon_y,\epsilon_y)] \\ &\qquad + q_Y^L 3\alpha[\mathcal{M}_0(\epsilon_y^L,\epsilon_y) - 2\mathcal{M}_1(\epsilon_y^L,\epsilon_y) - 2\alpha\mathcal{M}_0(\epsilon_y^L,\epsilon_y,\epsilon_y) + 4\alpha\mathcal{M}_1(\epsilon_y^L,\epsilon_y,\epsilon_y)] \ , \end{aligned} \tag{E.8}$$

$$\begin{aligned}\psi_{ASL} &= q_A^L \alpha \mathcal{M}_1(\epsilon_y^L,\epsilon_y) + q_X^L \alpha[(1-2\alpha)\mathcal{M}_1(\epsilon_y^L,\epsilon_y) + 2\alpha\mathcal{M}_2(\epsilon_y^L,\epsilon_y) + 2\alpha\mathcal{M}_1(\epsilon_y^L,\epsilon_y,\epsilon_y)] \\ &\quad + q_Y^L \alpha[\mathcal{M}_2(\epsilon_y^L,\epsilon_y) - \mathcal{M}_1(\epsilon_y^L,\epsilon_y)] \ , \end{aligned} \tag{E.9}$$

$$\begin{aligned}\psi_{XSL} &= q_A^L 3\alpha[2\alpha\mathcal{M}_1(\epsilon_y^L,\epsilon_y,\epsilon_y) - \mathcal{M}_1(\epsilon_y^L,\epsilon_y)] \\ &\quad + q_X^L 3\alpha[(2\alpha-1)\mathcal{M}_1(\epsilon_y^L,\epsilon_y) - 2\alpha\mathcal{M}_2(\epsilon_y^L,\epsilon_y) - 4\alpha^2\mathcal{M}_1(\epsilon_y^L,\epsilon_y,\epsilon_y) \\ &\qquad + 4\alpha^2\mathcal{M}_2(\epsilon_y^L,\epsilon_y,\epsilon_y) + 8\alpha^2\mathcal{M}_1(\epsilon_y^L,\epsilon_y,\epsilon_y,\epsilon_y)] \\ &\qquad + q_Y^L 3\alpha[\mathcal{M}_1(\epsilon_y^L,\epsilon_y) - \mathcal{M}_2(\epsilon_y^L,\epsilon_y) - 2\alpha\mathcal{M}_1(\epsilon_y^L,\epsilon_y,\epsilon_y) + 2\alpha\mathcal{M}_2(\epsilon_y^L,\epsilon_y,\epsilon_y)] \ , \end{aligned} \tag{E.10}$$

and

$$\begin{aligned}\psi_{YSL} &= q_A^L 3\alpha[\mathcal{M}_1(\epsilon_y^L,\epsilon_y) - \mathcal{M}_2(\epsilon_y^L,\epsilon_y)] \\ &\quad + q_X^L 3\alpha[(1-2\alpha)\mathcal{M}_1(\epsilon_y^L,\epsilon_y) + (4\alpha-1)\mathcal{M}_2(\epsilon_y^L,\epsilon_y) \\ &\qquad - 2\alpha\mathcal{M}_3(\epsilon_y^L,\epsilon_y) + 2\alpha\mathcal{M}_1(\epsilon_y^L,\epsilon_y,\epsilon_y) - 2\alpha\mathcal{M}_2(\epsilon_y^L,\epsilon_y,\epsilon_y)] \\ &\quad + q_Y^L \alpha[-3\mathcal{M}_1(\epsilon_y^L,\epsilon_y) + 6\mathcal{M}_2(\epsilon_y^L,\epsilon_y) - 2\mathcal{M}_3(\epsilon_y^L,\epsilon_y)] \ , \end{aligned} \tag{E.11}$$

where

$$q_A^L = S_{AL}\frac{\Delta y}{\eta} \ , \tag{E.12}$$

$$q_X^L = S_{XL}\frac{\Delta y}{\eta} \ , \tag{E.13}$$

and

$$q_Y^L = S_{YL}\frac{\Delta y}{\eta} \ . \tag{E.14}$$

REFERENCES

1. K. D. LATHROP, "Remedies for Ray Effects," *Nucl. Sci. Eng.*, **45**, 255 (1971).

2. B. G. PETROVIC and A. HAGHIGHAT, "Analysis of Inherent Oscillations in Multidimensional S_N Solutions of the Neutron Transport Equation," *Nucl. Sci. Eng.*, **124**, 31 (1996).

3. B. G. CARLSON and K. D. LATHROP, "Transport Theory—The Method of Discrete Ordinates," *Computing Methods in Reactor Physics*, Chap. 3, H. GREENSPAN, C. N. KELBER, and D. OKRENT Eds., Gordon and Breach, New York (1968).

4. K. D. LATHROP, "Spatial Differencing of the Transport Equation: Positivity vs. Accuracy," *J. Comput. Phys.*, **4**, 475 (1969).

5. W. F. WALTERS and R. D. O'DELL, "Nodal Methods for Discrete-Ordinates Transport Problems in (x,y) Geometry," *Proc. Int. Topl. Mtg. Advances Mathematical Methods for the Solution of Engineering Problems*, Munich, Germany, April 27–29, 1981, Vol. I, p. 115, American Nuclear Society (1981).

6. W. F. WALTERS, "Augmented Weighted-Diamond Form of the Linear-Nodal Scheme for Cartesian Coordinate Systems," *Nucl. Sci. Eng.*, **92**, 192 (1986).

7. W. F. WALTERS, "The Relation Between Finite Element Methods and Nodal Methods in Transport Theory," *Prog. Nucl. Energy*, **18**, 21 (1986).

8. E. W. LARSEN and R. E. ALCOUFFE, "The Linear Characteristic Method for Spatially Discretizing the Discrete Ordinates Equations in (X,Y)-Geometry," *Proc. Int. Topl. Mtg. Advances Mathematical Methods for the Solution of Engineering Problems*, Munich, Germany, April 27–29, 1981, Vol. I, p. 99, American Nuclear Society (1981).

9. K. A. MATHEWS and C. R. BRENNAN, "Exponential Characteristic Nonlinear Radiation Transport Method for Unstructured Grids of Triangular Cells," *Nucl. Sci. Eng.*, **126**, 264 (1997).

10. K. A. MATHEWS, "Adaptive Characteristic Spatial Quadratures for Discrete Ordinates Neutral Particle Transport—The Slab Geometry Case," *Transp. Theory Stat. Phys.*, **19**, 419 (1990).

11. K. A. MATHEWS and B. M. MINOR, "Adaptive Characteristic Spatial Quadratures for Discrete Ordinates Neutral Particle Transport—The Rectangular Cell Case," *Transp. Theory Stat. Phys.*, **22**, 655 (1993).

12. K. MATHEWS, G. SJODEN, and B. MINOR, "Exponential Characteristic Spatial Quadrature for Discrete Ordinates Radiation Transport in Slab Geometry," *Nucl. Sci. Eng.*, **118**, 24 (1994).

13. B. MINOR and K. MATHEWS, "Exponential Characteristic Spatial Quadrature for Discrete Ordinates Radiation Transport with Rectangular Cells," *Nucl. Sci. Eng.*, **120**, 165 (1995).

14. W. H. REED, T. R. HILL, F. W. BRINKLEY, and K. D. LATHROP, "TRIPLET: A Two-Dimensional, Multigroup, Triangular-Mesh, Planar Geometry, Explicit Transport Code," LA-5428-MS, Los Alamos National Laboratory (1973).

15. J. E. MOREL, J. E. DENDY, Jr., and T. A. WARING, "Diffusion-Accelerated Solution of the Two-Dimensional S_n Equations with Bilinear-Discontinuous Differencing," *Nucl. Sci. Eng.*, **115**, 304 (1993).